© 2020. Published by The Company of Biologists Ltd | Development (2020) 147, dev194530. doi:10.1242/dev.194530

RESEARCH ARTICLE

βIII spectrin controls the planarity of Purkinje cell dendrites by modulating perpendicular axon-dendrite interactions

Kazuto Fujishima[1,*], Junko Kurisu[1], Midori Yamada[1,2] and Mineko Kengaku[1,2]

ABSTRACT

The mechanism underlying the geometrical patterning of axon and dendrite wiring remains elusive, despite its crucial importance in the formation of functional neural circuits. The cerebellar Purkinje cell (PC) arborizes a typical planar dendrite, which forms an orthogonal network with granule cell (GC) axons. By using electrospun nanofiber substrates, we reproduce the perpendicular contacts between PC dendrites and GC axons in culture. In the model system, PC dendrites show a preference to grow perpendicularly to aligned GC axons, which presumably contribute to the planar dendrite arborization *in vivo*. We show that βIII spectrin, a causal protein for spinocerebellar ataxia type 5, is required for the biased growth of dendrites. βIII spectrin deficiency causes actin mislocalization and excessive microtubule invasion in dendritic protrusions, resulting in abnormally oriented branch formation. Furthermore, disease-associated mutations affect the ability of βIII spectrin to control dendrite orientation. These data indicate that βIII spectrin organizes the mouse dendritic cytoskeleton and thereby regulates the oriented growth of dendrites with respect to the afferent axons.

KEY WORDS: Dendrite development, Mouse, Neuron, Purkinje, SCA5, Spectrin, Spinocerebellar ataxia

INTRODUCTION

Accurate information processing through the neuronal network requires proper development of dendrite patterns, which determine the receptive field, afferent types and the number of synapses they form (London and Häusser, 2005). During development, neurons arborize their dendrites by a set of branch dynamics, including extension, branching and retraction, which are controlled by either cell-intrinsic programs or extrinsic cues from the surrounding tissue (Dong et al., 2015; Jan and Jan, 2010; Valnegri et al., 2015).

Cerebellar Purkinje cells (PCs) develop highly branched dendrites in a single parasagittal plane. The dendrites are innervated by parallel fiber axons of cerebellar granule cells (GCs), which run perpendicularly across the aligned PC dendrites along the coronal axis of the cerebellum. The planar dendrites with a space-filling and non-overlapping arrangement are a distinctive feature of PCs, which is thought to be advantageous for efficient network formation. For instance, planar dendrites connected with perpendicularly oriented axonal bundles contribute to maximization of possible synaptic connections with minimal redundancy (Cuntz, 2012; Wen and Chklovskii, 2008). Indeed, each PC dendrite contacts more than 100,000 parallel fibers in rodents (Napper and Harvey, 1988). PCs arborize their dendritic branches via dynamic remodeling during postnatal development (Fujishima et al., 2018; Joo et al., 2014; Kaneko et al., 2011; Kapfhammer, 2004; Sotelo and Dusart, 2009; Takeo et al., 2015; Tanaka, 2009). We have previously identified the basic rules of dendrite formation in PCs grown on coverslips (Fujishima et al., 2012). Typical fan-shaped branching structures were constructed by constant extension and dichotomous terminal branching. Furthermore, we have shown that retraction and stalling induced by dendro-dendritic contact (self-avoidance) play pivotal roles in the non-overlapping and space-filling distribution of branches (Fujishima et al., 2012; Kawabata Galbraith et al., 2018). Indeed, it has been shown that loss of cell-surface molecules such as clustered protocadherins and slit/robo, which recognize the contact between dendritic branches, affects the non-overlapping arrangement of PC dendrites (Gibson et al., 2014; Ing-Esteves et al., 2018; Kuwako and Okano, 2018; Lefebvre et al., 2012; Toyoda et al., 2014). Although these basic rules of dendritic growth explain the dendritic configuration, including the non-overlapping pattern on a two-dimensional (2D) substrate, they cannot illustrate how dendrites acquire the planar arrangement in three-dimensional tissue.

Unlike other planar dendrites, such as those of *Drosophila* dendritic arborization neurons that extend along the structural boundary (Han et al., 2012; Kim et al., 2012), PC dendrites grow in a plane with no obvious scaffolds in the cerebellum. Several lines of evidence suggest that the growth of PC dendrites is oriented in a direction perpendicular to the parallel fibers, which are formed earlier than the extension of PC dendrites (Altman and Anderson, 1972; Crepel et al., 1980; Nagata et al., 2006). The perpendicular growth seems to be involved in the flat dendrite arborization (Altman and Anderson, 1972; Crepel et al., 1980; Nagata et al., 2006; Sotelo and Dusart, 2009). Pioneering studies by Altman demonstrated that disruption of parallel fiber arrays via X-ray irradiation of the developing cerebellum led to the disruption and realignment of PC dendrites in a direction perpendicular to the misoriented parallel fibers (Altman, 1973). However, the molecular machinery underlying the dendrite growth perpendicular to the axonal arrays is largely unknown (Gao et al., 2011; Kim et al., 2014).

Spectrins are structural molecules that form a tetrameric complex with two α and two β subunits. Spectrin tetramers interact with actin filaments beneath the plasma membrane. Recent studies using super-resolution microscopy have revealed that spectrin, actin and their associated proteins form membrane periodic skeletal (MPS) structures lining the circumference of the axons and dendrites (D'Este et al., 2015; Han et al., 2017; Vassilopoulos et al., 2019; Xu et al., 2013). In the MPS structures, ring-like structures of actin are connected by spectrin tetramers with a periodicity of ∼190 nm. Alternatively, spectrin and associated proteins can form a 2D polygonal lattice structure in the soma or dendrites, reminiscent of

---

[1]Institute for Integrated Cell-Material Sciences (KUIAS-iCeMS), Kyoto University, Kyoto 606-8501, Japan. [2]Graduate School of Biostudies, Kyoto University, Kyoto 606-8501, Japan.

*Author for correspondence (fujishima@icems.kyoto-u.ac.jp)

K.F., 0000-0001-6374-4486

Handling Editor: Paola Arlotta
Received 1 July 2020; Accepted 4 November 2020

those found in erythrocytes (Han et al., 2017). These structures are considered to have multiple functions, such as the maintenance of membrane stiffness and/or elasticity (Krieg et al., 2017) and acting as diffusion barriers to membrane molecules (Albrecht et al., 2016).

βIII spectrin, one of the spectrin β subunits, is highly expressed in the PC dendrites and soma. βIII spectrin (*Sptbn2*) has been identified as a gene responsible for spinocerebellar ataxia type 5 (SCA5), which manifests as a progressive dysfunction of motor coordination (Ikeda et al., 2006). PCs in SCA5 patients and βIII spectrin knockout animals display aberrant dendrite morphologies owing to abnormal arbor development and maintenance (Gao et al., 2011; Ikeda et al., 2006). Notably, PCs in the knockout mouse exhibit a defect in flat dendrite arborization (Gao et al., 2011), implicating βIII spectrin in the regulation of the orientation of dendrite growth. The loss of βIII spectrin leads to the mislocalization and/or diminished level of neurotransmitter receptors and transporters, which might cause the progressive neurodegeneration via excitotoxicity (Armbrust et al., 2014; Perkins et al., 2010; Stankewich et al., 2010). However, the mechanisms by which βIII spectrin controls dendrite development remain elusive.

Here, we show that βIII spectrin is indispensable for the directional PC dendrite arborization perpendicular to parallel fibers, which is a prerequisite for the flat dendrite formation. We recapitulated a 2D model of the orthogonal interaction between the dendrite and axonal bundles by using nanofibers as artificial scaffolds to reproduce parallel fiber arrays *in vitro*. We demonstrated that βIII spectrin-deficient PCs failed to form dendrites perpendicular to axonal bundles. Super-resolution observations confirmed the repeated lattice-like βIII spectrin structures in PC dendrites. Loss of βIII spectrin caused abnormal cytoskeletal dynamics and misoriented dendrite growth. Our data provide insights into the role of βIII spectrin in controlling the perpendicular connectivity of dendrites and axons to form planar dendrites.

RESULTS

βIII spectrin is required for a cell-autonomous mechanism of planar dendrite arborization in PCs

Earlier studies have demonstrated that the planarity of PC dendrites is disturbed in loss-of-function mutants of βIII spectrin (Gao et al., 2011). We first confirmed the cell-autonomous role of βIII spectrin in PC dendrite formation by short hairpin RNA (shRNA) knockdown in the wild-type background *in vivo*. We used a plasmid encoding an shRNA targeting βIII spectrin that efficiently knocks down βIII spectrin expression in PCs in a dissociation culture (Fig. S1). Dendrites of βIII spectrin-knockdown cells exhibited the characteristic tapering shape seen in knockout cells (Gao et al., 2011). Besides, there was no notable difference in dendritic shape between control (ctr) and knockdown cells. We delivered the plasmid sparsely into PC precursors via *in utero* electroporation at embryonic day (E) 11.5. Consistent with previous observations using βIII spectrin knockout mice, we observed almost no differences in the total length of dendrites between control and knockdown cells at postnatal day (P) 14 (Fig. 1A-C). Compared with the normal planar dendrites in control, knockdown PCs exhibited misoriented dendrites that extended away from the main dendritic plane (Fig. 1A,B), similar to those in knockout animals (Gao et al., 2011). Quantitative analysis revealed that the number of dendritic branches extruded away from the main plane was significantly increased in knockdown PCs (Fig. 1A,B,D; Fig. S2; see Materials and Methods), suggesting that a cell-autonomous function of βIII spectrin is necessary for the planar dendrite formation.

Recapitulation of 2D perpendicular contact between PC dendrites and GC axons using artificial nanofibers *in vitro*

Next, we examined the mechanism underlying the effect of βIII spectrin deficiency on dendrite planarity. Considering that flat dendrites are closely aligned with neighboring PCs (Fig. 2A), it seems unlikely that gradients of guidance molecules instruct such dendritic configurations. It has previously been suggested that PC dendrites grow perpendicularly to GC axons (Nagata et al., 2006). If so, dendrites will extend in parasagittal planes perpendicular to the bundle of parallel fibers (GC axons) that run along the coronal axis (Fig. 2B, left). We thus speculated that βIII spectrin might be involved in dendrite growth perpendicular to GC axons.

To test this hypothesis, we first confirmed whether normal PC dendrites preferentially grow perpendicularly to GC axons. We established a simplified model in which parallel GC axons are recapitulated in 2D spaces (Fig. 2B, right). We used electrospun polycaprolactone nanofibers, which have been used to navigate axonal extensions in culture (Hyysalo et al., 2017). We plated dissociated cells from P0 cerebella on aligned or randomly oriented nanofibers. GCs were labeled with green fluorescent protein (GFP) and identified by the expression of the GC marker Pax6 (Engelkamp et al., 1999). As expected, GC axons ran parallel to each other on aligned nanofibers (arrowheads in Fig. 2C), whereas they extended randomly on non-oriented nanofibers (arrowheads in Fig. 2E).

We previously reported that PCs in dissociated cultures initiate dendrites at ∼8 days *in vitro* (DIV) and extend branches radially until at least 14 DIV (Fujishima et al., 2012). Likewise, PC dendrites on the randomly oriented nanofibers were observed to grow radially, with no directional preference (Fig. 2F). By contrast, the distribution of PC dendrites on aligned nanofibers was highly biased toward the direction perpendicular to fibers, supporting the notion that PC dendrites grow perpendicularly to GC axons (Fig. 2D). Indeed, quantitative analysis revealed that the majority of dendritic segments oriented perpendicular to aligned fibers (polar histogram: dendrite orientation in Fig. 2D; see Materials and Methods; Fig. S3). The perpendicular growth was specific to PC dendrites, because PC axons grew parallel to GC axons (Fig. 2D). Furthermore, GC dendrites grew in a random orientation on aligned fibers (Fig. 2C). These results suggest that the perpendicular interaction is not ubiquitous but is specific to certain synaptic partners, including PC dendrites and GC axons.

To verify that PC dendrites are navigated by GC axons but not by nanofibers, we confirmed the interactions between PC dendrites and GC axons without nanofibers (Fig. S4A). We prepared microexplants of the external granule layer populated with differentiating GCs from the P2 cerebellum (Kawaji et al., 2004; Nagata and Nakatsuji, 1990). Isolated PCs were co-cultured at 1 DIV on the GC axons that extended radially from the explant. We confirmed that PCs developed dendrites perpendicular to the radially extended GC axons at 10 DIV (Fig. S4A), consistent with a previous report (Nagata et al., 2006). Surface rendering showed close apposition of the dendrites and axons (Fig. S4B). These results suggest that direct PC dendrite-GC axon interaction determines the dendrite orientation.

To exclude the possibility that the nanofibers act as scaffolds for PC dendrite growth, we prepared PC cultures with GCs of different densities on nanofibers (Fig. S5). Although PCs established perpendicular dendrites in high- and medium-density cultures, they could not grow dendrites on free nanofibers devoid of GC axons in a low-density culture, suggesting that nanofibers do not serve as growth scaffolds (Fig. S5A,B). Taken together, we conclude that PC dendrites grow perpendicular to GC axons.

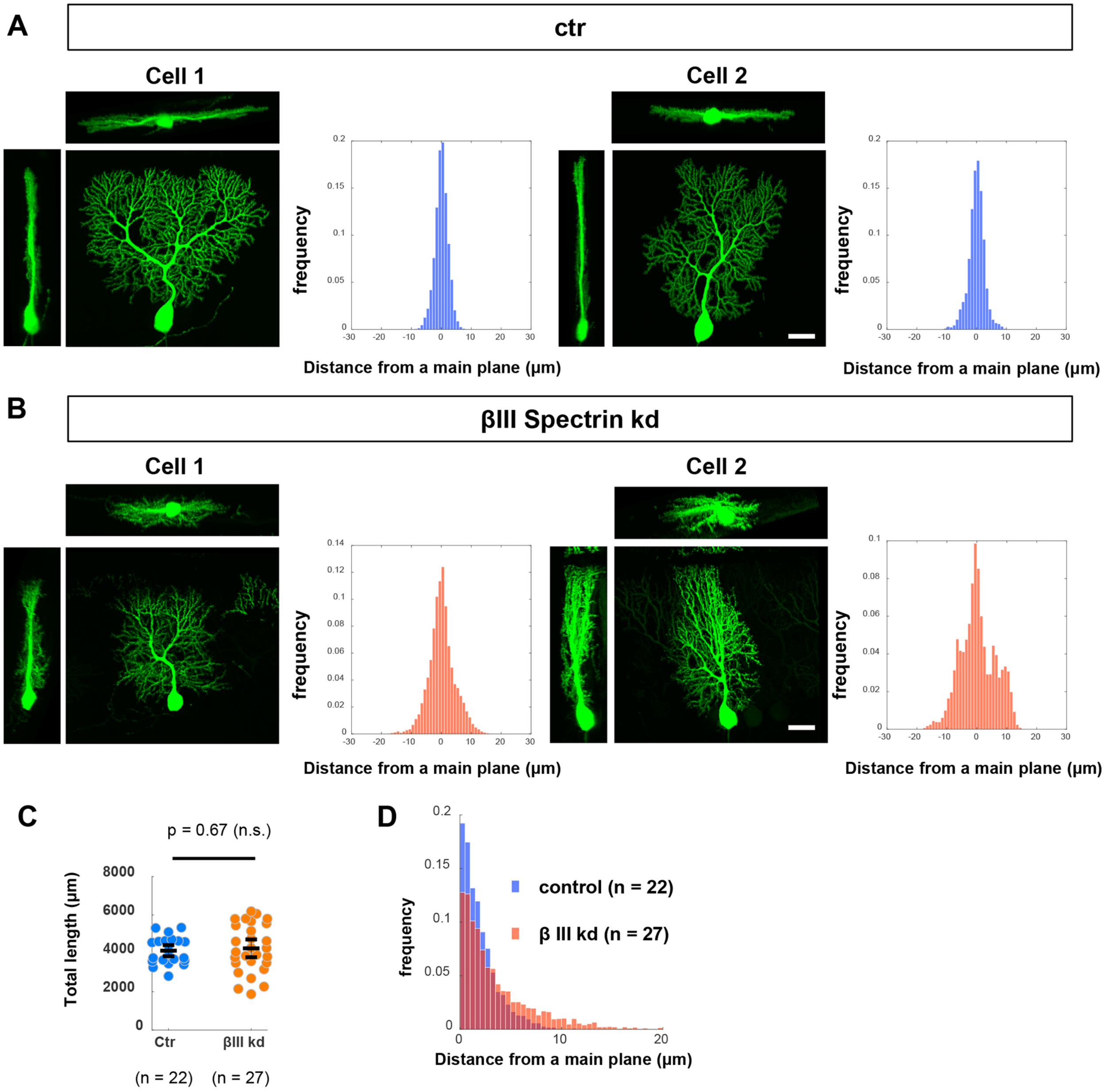

Fig. 1. A cell-autonomous role of βIII spectrin in the planar dendrite formation *in vivo*. (A,B) Morphology of PCs expressing the GFP/shRNA-control (A) or GFP/shRNA-βIII spectrin plasmid (B) in P14 sagittal sections. Top, front (sagittal) and side (coronal) views were taken from the three-dimensionally reconstructed images. Histograms show the proportions of dendritic segments locating at the indicated distances from the main dendritic plane. (C) Quantification of total dendritic length at P14. Statistical analysis: Welch's *t*-test. (D) Proportions of dendritic segments locating at the indicated distances from the main dendritic plane. P=2.7×10^{-46}, two-sample Kolmogorov–Smirnov test. Scale bars: 20 μm in A,B.

Knockdown of βIII spectrin interferes with directed dendrite growth perpendicular to GC axons

To examine whether βIII spectrin is required for the perpendicular interaction between PC dendrites and GC axons, we introduced shRNA plasmids to PCs and plated them on nanofibers. In contrast to the dendrites perpendicular to GC axons observed in control cells, a significant proportion of the branches in βIII spectrin-knockdown dendrites extended in different orientations (Fig. 3A). Quantitative morphometry revealed that the total length and number of branches were increased in knockdown cells, suggesting excess misoriented branch formation (Fig. 3B,C). This is inconsistent with the observations *in vivo*, where the total length was not affected by the loss of βIII spectrin (Fig. 1). We attribute this discrepancy to a homeostatic mechanism of dendritic growth, which adjusts the size of PC dendrites to match the amount of available neurotrophic factors from afferent axons *in vivo* (Joo et al., 2014). Co-expression of shRNA-resistant βIII spectrin reversed the changes in dendrite orientation, total length and number of branches, negating the off-target effects (Fig. 3A-C, βIII kd+rescue). Furthermore, the CRISPR/Cas9-based βIII spectrin knockout dendrites exhibited similar misoriented phenotypes (Fig. S6). These results indicate that βIII spectrin is required for directed dendrite formation perpendicular to GC axons.

Spectrin molecules form tetrameric complexes composed of α and β subunits, and the loss of α subunits destabilizes β subunits in embryonic tissue (Stankewich et al., 2011). Among α-spectrin subtypes, αII spectrin is most abundant in non-erythrocytic cells (Cianci et al., 1999; Winkelmann and Forget, 1993). Indeed, αII spectrin was strongly expressed in PC somata and dendrites, similar

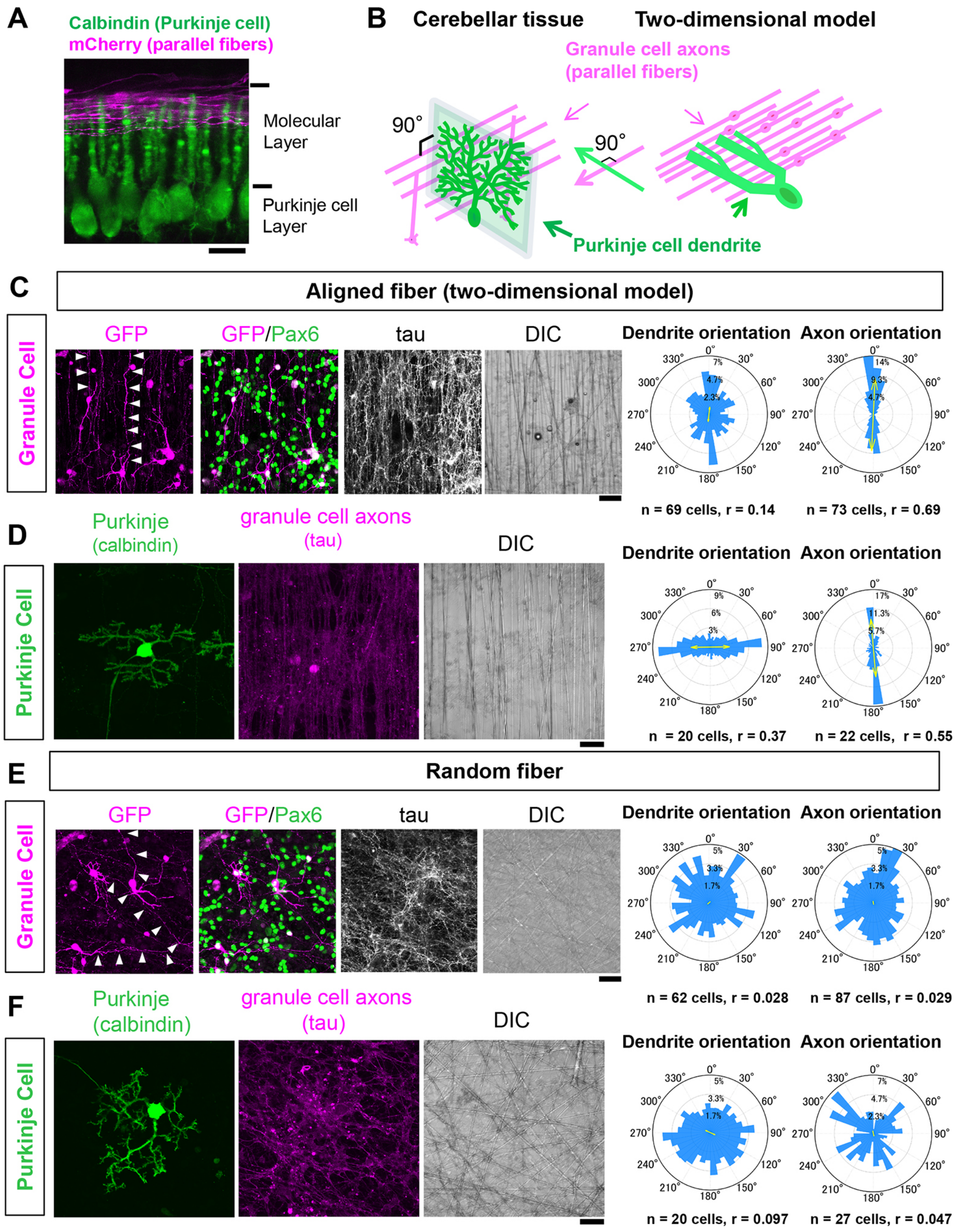

Fig. 2. Reconstruction of perpendicular interactions between PC dendrites and GC axons using artificial nanofibers. (A) PCs (calbindin) and parallel fibers (mCherry, introduced by *in vivo* electroporation) in a P11 coronal section. (B) Schematic diagrams illustrating the arrangement of PC dendrites and parallel fibers in the cerebellum and in a 2D model. (C-F) Representative images of GCs (C,E) and PCs (D,F) grown on nanofibers (C,D, aligned; and E,F, random). In C,E, Pax6-positive GC morphologies were visualized with GFP. Axons were stained with tau. In D, F, PCs were visualized by calbindin staining. Polar histograms indicate the angular distribution of the axons or dendrites of GCs or PCs. The mean vector is shown with the yellow arrow, and its length is indicated as r. Scale bars: 30 µm in A,C-F.

to βIII spectrin (Fig. 3D). We found that the knockdown of either αII or βIII spectrin dramatically reduced both proteins in PCs, suggesting the interdependency of the molecules in stabilization of the spectrin complex (Fig. 3D). Accordingly, αII spectrin knockdown disrupted planar arborization *in vivo* (Fig. 3E) in addition to biased dendrite organization on aligned nanofibers (Fig. 3F). Thus, these results indicate that the αII/βIII spectrin complex regulates PC dendrite orientation.

Loss of βIII spectrin causes aberrant branch formation

We have previously demonstrated that the non-overlapping arrangement of PC dendrites is achieved by contact-dependent branch retraction (Fujishima et al., 2012). Thus, the perpendicular dendrites on nanofibers might be attributed either to biased outgrowth (extension and branch formation) in the perpendicular direction or to the biased retraction of misoriented branches. To distinguish between these possibilities, we performed time-lapse observations of growing dendrites on aligned nanofibers. We traced the outgrowth of PC dendrites (~0.7 µm/h) every 3 h for several days from 8 DIV, when dendrite formation was initiated in the culture (Fujishima et al., 2012). Control PCs continuously grew their dendrites by extension and branch formation perpendicular to the GC axon orientation (Fig. 4A,B). Next, we measured the orientation of retracted branches. Dendritic retractions were triggered by collisions of growing dendritic tips, consistent with our previous report (Fujishima et al., 2012). Of all dendritic retractions observed in control PCs, ~86% were induced after obvious dendritic collisions. In addition, ~73% of branches were eliminated after a collision (Fig. 4D). Disorienting branches were eliminated with high probability because they had more chance of contact with other branches, but perpendicular branches were also retracted when they collided with other growing branches (Fig. 4C).

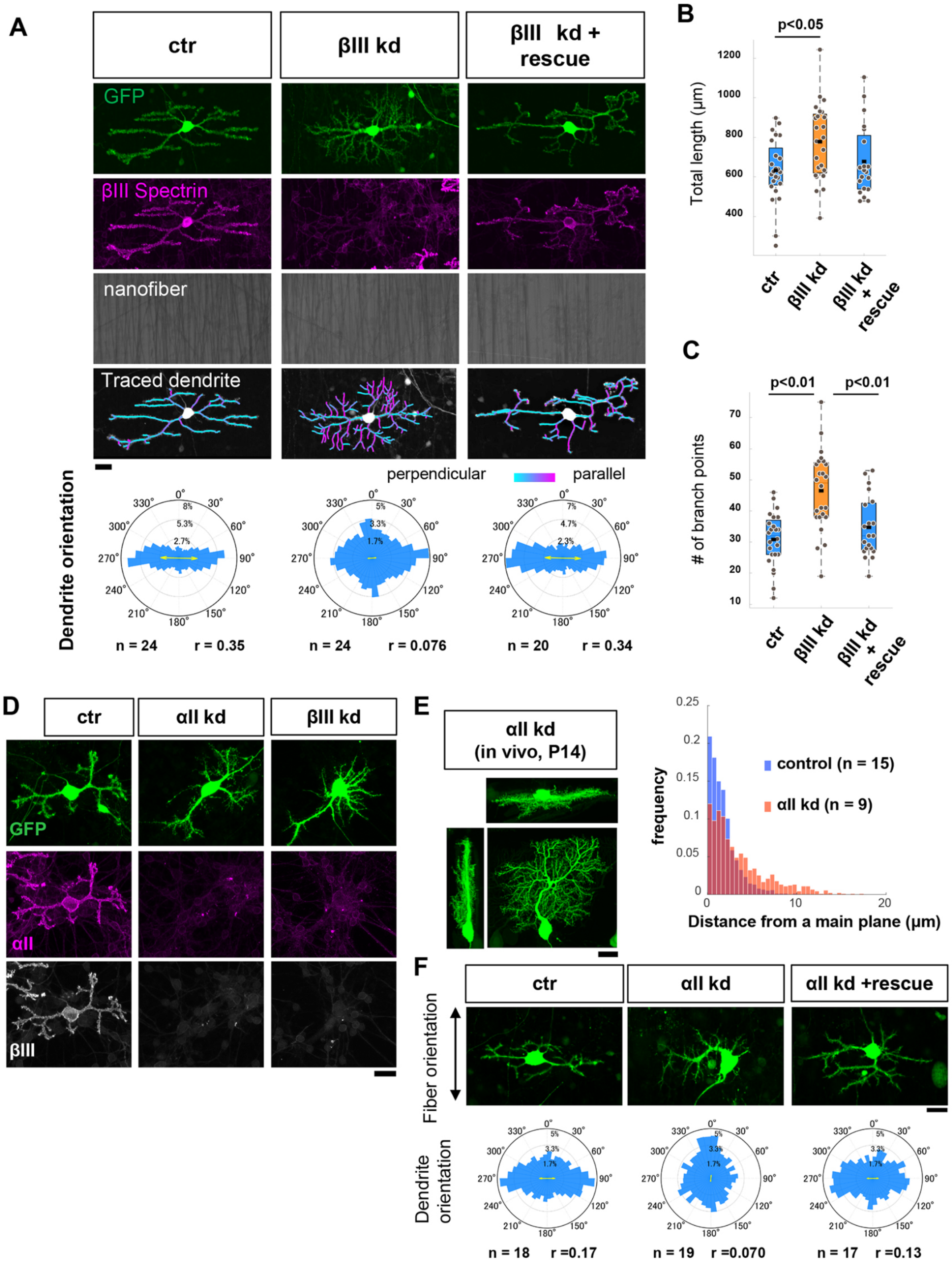

Fig. 3. Disruption of perpendicular dendrite growth via the knockdown of βIII spectrin. (A) Morphology of PCs transfected with GFP/shRNA control (ctr), GFP/shRNA-βIII spectrin (βIII kd) and GFP/shRNA-βIII spectrin with shRNA-resistant βIII spectrin (βIII kd+rescue) grown on aligned fibers (12 DIV). Traced dendrites are pseudocolored based on the angles between the dendritic segments and fibers. Polar histograms indicate angular distributions of dendritic segments. $P=6\times10^{-16}$ for ctr versus βIII kd, $P>0.5$ for ctr versus rescue, and $P=6\times10^{-16}$ for βIII kd versus rescue (Watson–Wheeler test with Bonferroni correction). (B,C) Quantification of total dendritic length (B) and number of branches (C). Statistical analysis: ANOVA followed by the Tukey–Kramer post hoc test. (D) αII and βIII spectrin signals in PCs transfected with GFP/shRNA-control (ctr), GFP/shRNA-αII spectrin (αII kd) and GFP/shRNA-βIII (βIII kd). (E) Morphology of PCs transfected with GFP/shRNA-αII spectrin (αII kd) in P14 sagittal section. The histogram shows the proportions of dendritic segments locating at the indicated distance from the main dendritic plane. $P=2.2\times10^{-39}$, two-sample Kolmogorov–Smirnov test. (F) Top panels, morphology of PCs transfected with GFP/shRNA-control (ctr), GFP/shRNA-αII spectrin (αII kd) and GFP/shRNA-αII spectrin plus shRNA-resistant αII spectrin (αII kd+rescue) grown on aligned nanofibers. Bottom panels, angular distribution of dendritic segments. Scale bars: 20 μm in A,D-F.

Therefore, we concluded that the perpendicular dendrite orientation in control PCs was likely to be attributable to biased dendritic growth, although the elimination of disoriented branches might contribute to some extent.

In βIII spectrin-knockdown PCs, the fraction of parallel-growing dendritic terminals was markedly increased (Fig. 4A,B). Similar to control PCs, most of the dendritic retractions (~90%) in knockdown cells occurred after the dendritic collisions. However, the frequency

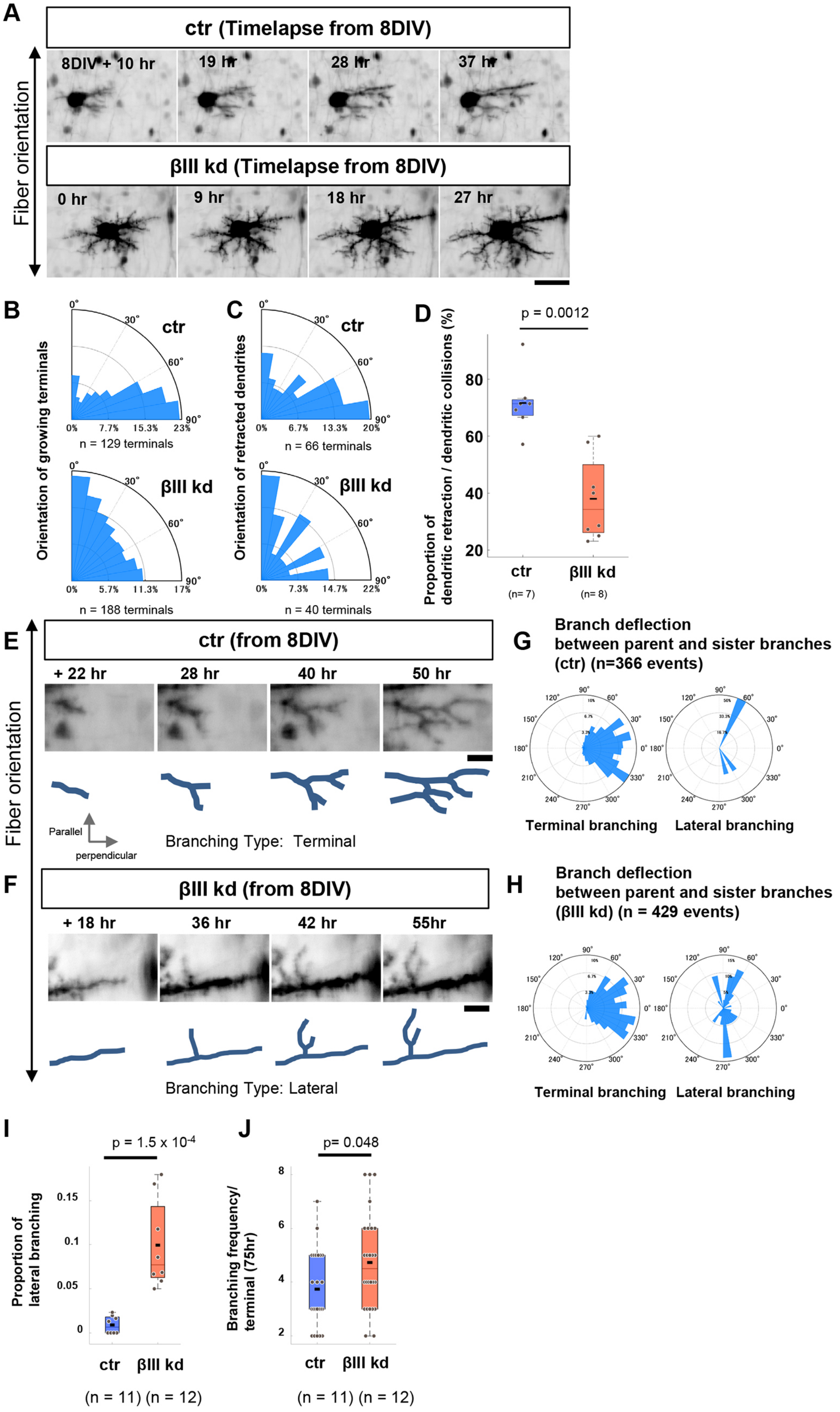

Fig. 4. Analysis of PC dendrite dynamics on aligned nanofibers. (A) Time-lapse images of developing dendrites in GFP/shRNA-control (ctr) or GFP/shRNA-βIII spectrin (βIII kd) PCs growing on aligned nanofibers. (B,C) Angular distributions of growing dendritic terminals (B) or retracted dendrites (C). (D) The number of retracted dendrites per cell during the 75 h time-lapse observation. (E,F) Magnified views of time-lapse images of control (E) or βIII kd (F) dendrites, focusing on the branch formation. Images show the examples of terminal branching (E) or lateral branching (F) observed in control or βIII kd cells, respectively. Branch formation more than 15 µm away from the terminal was defined as lateral branching. (G,H) Deflection angles between parent and sister branches at terminal branching (left) or lateral branching (right) in ctr (G) and βIII kd cells (H). (I) The proportion of lateral branching. (J) Branching frequency of growing dendrites. Statistical analysis: Wilcoxon rank-sum test in D,I,J. Scale bars: 40 µm in A; 10 µm in E,F.

of dendrite retraction after a collision was reduced to 39%, suggesting that contact-dependent dendritic retraction is dysregulated in knockdown cells (Fig. 4D). However, the orientation of retracted dendrites was strongly biased parallel to axons, refuting that the increase in misoriented dendrites in knockdown cells was caused by the suppression of retraction of errant arbors. Therefore, we focused on how βIII spectrin deficiency leads to the dysregulation of growth orientation.

Our previous studies have shown that PCs form dendritic branches primarily via the bifurcation of growing terminals (terminal branching), whereas they rarely extend collaterals from the shaft (lateral branching) (Fujishima et al., 2012). Accordingly, control dendrites on aligned fibers mainly displayed terminal branching (Fig. 4E,I). By contrast, lateral branching was increased by more than 10-fold in βIII spectrin-knockdown dendrites (Fig. 4F,I), although the branching frequency was only slightly altered (Fig. 4J). The deflection angle between the bifurcated terminal branches ranged within approximately ±30°, whereas that of lateral branching was greater than 60° in both the control and knockdown dendrites (Fig. 4G,H). These results suggest that βIII spectrin regulates the perpendicular dendrite growth by inhibiting lateral branching. Thus, the frequent lateral branching might contribute to the increase in misoriented dendrites in the βIII spectrin-deficient cells.

Lateral branch formation in βIII spectrin-knockdown dendrites

We next observed how dendritic planarity was affected in βIII spectrin-knockdown cells *in vivo*. Control dendrites transfected with GFP aligned in a parasagittal plane in the molecular layer parallel to the neighboring PC dendrites (Fig. 5A,B). These PCs rarely exhibited dendritic branches growing in lateral (coronal) directions. Neighboring dendrites were separated by gaps of ∼1-3 µm, showing minimal crossing with adjacent branches. Similar to control PCs, the main dendritic arbors of knockdown PCs were mostly parallel to neighboring dendrites in coronal sections (Fig. 5A,B, βIII kd), although some dendrites bent or tilted into incorrect planes (white arrows in Fig. 5A). Notably, knockdown dendrites exhibited an increased number of laterally oriented branches growing into the territories of the neighboring PC dendrites (yellow arrows in Fig. 5A,C). These misoriented branches often turned and extended parasagittally into the gaps between PC dendrites (yellow arrowhead in Fig. 5A). These misoriented lateral branches are likely to contribute to the disruption of planar dendrites in βIII spectrin-deficient PCs.

It has been demonstrated that the growing PC dendrites are covered with numerous dendritic protrusions, including dendritic filopodia and immature spines (Kawabata Galbraith et al., 2018; Shimada et al., 1998). Given that dendritic protrusions are known to serve as branch precursors in some neurons, we next analyzed the protrusions in PCs with or without βIII spectrin expression. Control dendrites presented numerous protrusions emanating from the shaft, with a mean length of 1.48±0.04 µm (mean±s.e.m., *n*=231) (Fig. 5D,E). By contrast, βIII spectrin-knockdown dendrites exhibited significantly longer protrusions (2.21±0.17 µm, *n*=102) at a lower density, in agreement with previous studies (Fig. 5D-F) (Efimova et al., 2017; Gao et al., 2011). Notably, some protrusions in βIII spectrin-knockdown cells were abnormally elongated (>5 µm) in lateral directions away from the main sagittal plane of the dendritic shaft (arrows in Fig. 5D,G). These long lateral protrusions seemed to serve as precursors of the ectopic lateral branches in βIII spectrin-deficient cells.

Abnormal formation of dendritic protrusions in βIII spectrin-knockdown dendrites

To analyze the implications of βIII spectrin in the formation of dendritic protrusions and branches, we observed the dendritic structures in neurons grown on aligned nanofibers. Control PCs bore highly dense protrusions that covered the lateral surface of the dendritic shaft, similar to those observed *in vivo* (Fig. 6A). These protrusions expressed glutamate receptor δ2 (GluD2), which functions as a synaptic glue by binding with presynaptic neurexin/Cbln1 in GC axonal terminals (Matsuda et al., 2010; Uemura et al., 2010), suggesting that these protrusions are dendritic spines or spine precursors (Fig. 6A).

Compared with the control PCs, the distal dendrites of βIII spectrin-knockdown cells were significantly thinner (ctr, 1.80±0.15 µm, *n*=19; βIII kd, 0.90±0.06 µm, *n*=22, mean±s.e.m., $P=7\times10^{-6}$, Student's *t*-test) (Fig. 6B). In contrast to the dendritic protrusions in control cells, which presented a relatively constant length of 1-3 µm, those in knockdown cells presented various lengths at a lower density, with an average length that was significantly longer than that in control cells (Fig. 6C,D). We found some abnormally elongated protrusions of nearly 10 µm in knockdown dendrites that extended parallel to the orientation of GC axons. The extremely long protrusions exhibited multiple GluD2 puncta that were irregularly arranged along their lengths [Fig. 6B, region of interest (ROI)2]. The orientation of the protrusions in the control and knockdown dendrites was mostly parallel to GC axons (Fig. 6E). Other short protrusions often appeared wider at their bases, reminiscent of the shaft synapses with deficient neck formation observed in βIII spectrin-deficient hippocampal neurons (Fig. 6B, ROI1) (Efimova et al., 2017). We also observed ectopic GluD2 puncta on the dendritic shaft. These results suggest that βIII spectrin is required for shaping dendritic protrusions and that its loss results in the conversion of those protrusions to either spineless shaft synapses or abnormally oriented branches extending along the GC axons (Fig. 6F).

We next analyzed the subcellular localization of βIII spectrin in growing dendrites in PCs cultured on coverslips. Consistent with previous reports (Efimova et al., 2017; Gao et al., 2011), βIII spectrin was strongly localized on the surface of the dendritic shaft and the protrusion base, whereas it was excluded from the protrusion tips (Fig. 6G,H). Actin showed an inverse gradient along the protrusions such that it was densely localized at the tip and sharply declined in the base of the protrusion and the shaft (Fig. 6H,I). By contrast, in βIII spectrin-knockdown PCs, actin was more widely distributed along the entire length of both long and thin (Fig. 6J, type 1) and short and stubby (Fig. 6J, type 2) protrusions and was often dispersed in the shaft of distal dendrites (Fig. 6J, type 1; Fig. 6K). These results imply that βIII spectrin might be involved in the formation of the structural boundary between the dendritic shaft and protrusions that confines actin filaments within protrusions.

Membrane periodic skeletal structure formed by βIII spectrin

Super-resolution microscopy has revealed that the spectrin-actin complex forms MPS structures, which might function as a barrier to diffusion for membrane proteins (Albrecht et al., 2016; Leite et al., 2016). Using stimulated emission depletion microscopy (STED), we confirmed the existence of MPS-like repeated structures composed of βIII spectrin in the shaft of developing PC dendrites (Fig. S7A,C, ROI1). The average interval of the repeated structures was 186±5 µm (Fig. S7D), consistent with previous studies (Xu et al., 2013). Actin rings were not clearly observed in the structures, probably owing to very low actin signals in the shafts compared with the dendritic filopodia (data not shown; Fig. 6H). Repeated βIII spectrin signals were also observed along the narrow corridor of the protrusion neck (Fig. S7B,C, ROI2 and ROI3) with an interval of 187±5 µm (Fig. S7D). The repeated structures were not continuous but were often interrupted by irregularly arranged subsets, consistent with previous observations demonstrating the lower propensity for repeated structure formation in dendrites (Fig. S7E,F) (D'Este et al., 2015; Han et al., 2017). Thus, βIII spectrin formed random meshwork or repeated structures in dendritic shafts and filopodial bases.

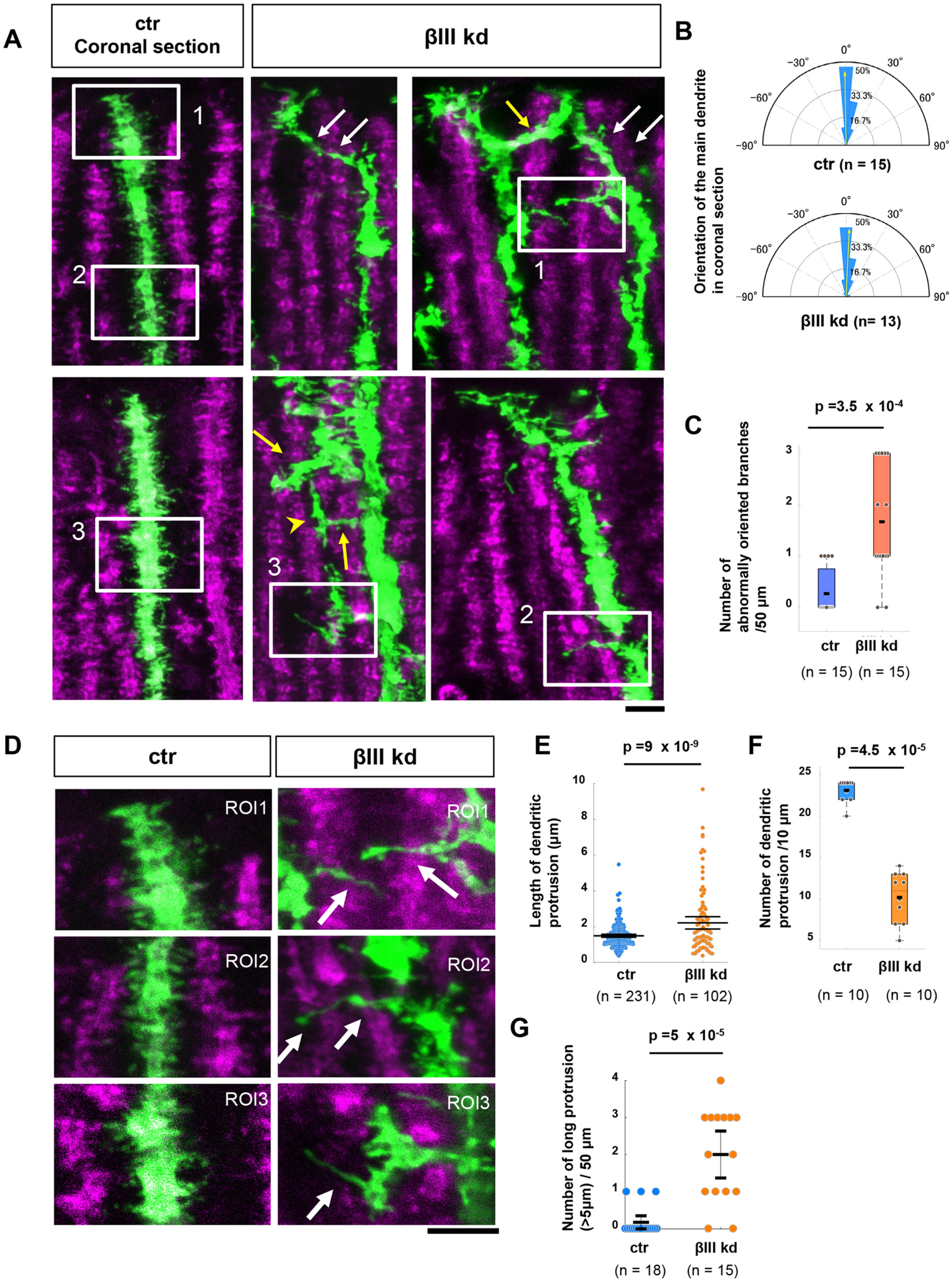

Fig. 5. βIII spectrin knockdown induces the extension of laterally oriented branches. (A) Growing dendritic arbors in PCs transfected with GFP/shRNA-control (ctr) or GFP/shRNA-βIII spectrin (βIII kd) in the vermis region in P14 coronal slices. βIII spectrin signals are shown in magenta. (B) Angular distribution of the main dendritic arbor. (C) The number of laterally oriented branches extruded from the main dendrites. (D) Images are magnified views of the insets in A. (E) Length of dendritic protrusions. (F) Number of dendritic protrusions per 10 µm of the dendritic segment. (G) The number of abnormally long (more than 5 µm) dendritic protrusions per 50 µm of the dendritic segment. Statistical analyses: Wilcoxon rank-sum test in C; Student's *t*-test in E-G. Scale bars: 5 µm in A,D.

βIII spectrin suppresses microtubule entry into dendritic protrusions

It has previously been demonstrated using young hippocampal neurons that the transition from filopodia to neurites is triggered by microtubule invasion into the filopodia after local actin remodeling (Dent et al., 2007; Flynn et al., 2012). To test whether βIII spectrin contributes to blocking microtubule entry into dendritic protrusions, we monitored microtubule polymerization in dendrites by transfecting end-binding protein 3 fused with enhanced green fluorescent protein (EB3-EGFP), a plus-end marker of dynamic microtubules. We analyzed the growing

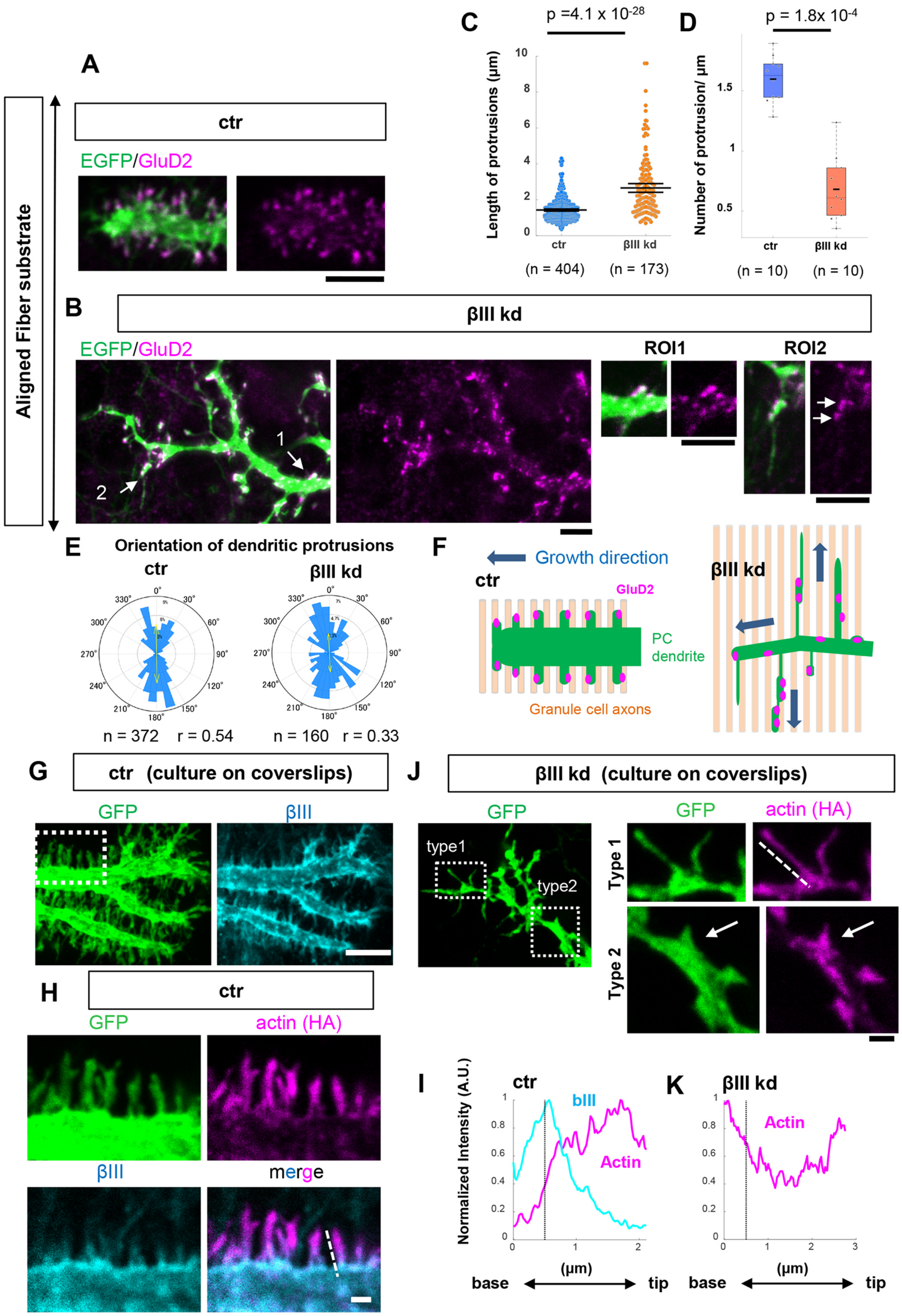

Fig. 6. Abnormal extension of dendritic protrusions is induced by the loss of βIII spectrin. (A,B) Representative images of the growing dendritic terminals of PCs transfected with GFP/shRNA-control (A) or GFP/shRNA-βIII spectrin (B). Cells were cultured on aligned nanofibers and stained with postsynaptic GluD2 (magenta) at 10 DIV. ROI1 and ROI2 are magnified views of the regions indicated by arrows 1 and 2 in the left image. (C) Length of dendritic protrusions. (D) Number of dendritic protrusions per micrometer. Statistical analysis: Wilcoxon rank-sum tests. (E) Orientation of dendritic protrusions. (F) Schematic explanation of growing dendrites (green) in control or βIII kd PCs on aligned GC axons (light orange). (G) Localization of βIII spectrin (cyan) in the growing dendrite in a control PC grown on a coverslip. (H) Magnified views of actin and βIII spectrin signals in the dendritic protrusions in the boxed region of G. HA-actin was transfected to visualize actin signals. (I) Intensity profiles of βIII spectrin and actin along the dotted line in H. The black dotted line in the graph indicates the boundary between the protrusion and shaft. (J) Left: representative image of the growing dendrites of GFP/βIII spectrin kd PCs grown on coverslips. Right: magnified views of actin signals in the dendritic protrusions (type 1, thin and long; type 2, short and stubby) in βIII kd cells. (K) Intensity profiles of actin along the dotted line in J. Scale bars: 5 µm in A,B,G,J (left panel); 1 µm in H,J (right panels).

dendritic terminals (within 10 µm from the terminal) and more proximal dendrites (more than 10 µm away from the terminal) separately to examine the regional difference in EB3 dynamics.

In control PCs, 48±5% (mean±s.e.m., 226 protrusions from 18 dendrites) of dendritic protrusions around the growing terminal were targeted by EB3-EGFP within 150 s of observation (Fig. 7A,C). By contrast, a significantly lower proportion of protrusions were invaded by EB3 in proximal dendrites (5±2%, 149 protrusions from 11 dendrites), in line with the notion that microtubule entry into filopodia triggers neurite extension at dendritic tips.

We found that βIII spectrin knockdown significantly increased the proportion of EB3-targeted protrusions in proximal regions (41±6%, 91 protrusions from 10 dendrites) (Fig. 7B,C), whereas only a slight increase was observed in the distal area (67±4%, 102 protrusions from 13 dendrites). These data support the idea that βIII spectrin interferes with microtubule invasion into protrusions in proximal dendrites. We often observed that the dendritic protrusions targeted by EB3 puncta extended aberrantly (Fig. 7D). Motility of those protrusions was immediately suppressed by treatment with the microtubule depolymerizer colchicine (Fig. S8), supporting that

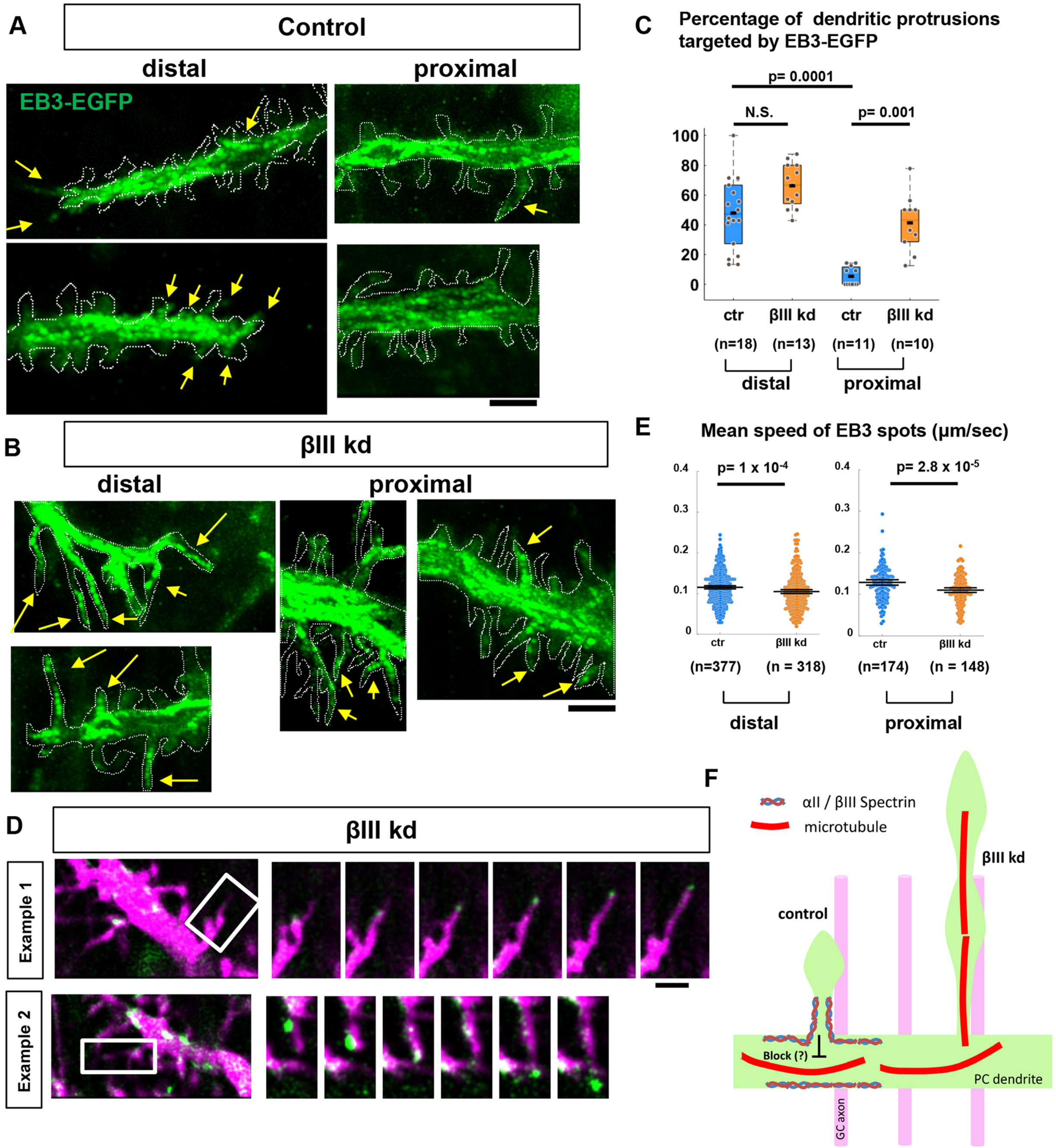

Fig. 7. The invasion of EB3 into dendritic protrusions is facilitated by the loss of βIII spectrin. (A,B) Time-lapse imaging of EB3-EGFP in the dendrites of PCs transfected with mCherry/shRNA-control (A) or mCherry/shRNA-βIII spectrin (B). Images are the maximum projections of EB3-EGFP spots during 150 s of observation. Distal (left) and proximal (right) dendritic regions were recorded every 3 s. Dotted lines indicate the contour of dendrites (mCherry). EB3-EGFP signals in dendritic protrusions are indicated by arrows. (C) The proportion of filopodia targeted by EB3-EGFP within 150 s of observation. (D) Example of filopodial extension associated with EB3-EGFP signals at the proximal dendrite region in βIII kd cells. Right panels show time-series images (12 s intervals) of boxed regions in the left images. (E) Speed of EB3 spots traveling within PC dendrites. (F) Schematic hypothesis of the function of βIII spectrin in the regulation of microtubule dynamics. Statistical analyses: Steel–Dwass test in C; Wilcoxon rank-sum test in E. Scale bars: 3 μm in A,B; 2 μm in D.

microtubule entry drives aberrant elongation of protrusions in knockdown cells. The speed of the EB3 movement was instead slightly downregulated in knockdown cells, refuting that excessive microtubule entry in knockdown cells was caused by increased microtubule polymerization activity (Fig. 7E). These results suggest that βIII spectrin controls directed dendritic arborization by suppressing microtubule invasion and ectopic branch formation from proximal dendritic protrusions (Fig. 7F).

Mutations causing SCA5

Mutations in βIII spectrin are known to cause SCA5. We wondered whether the disease mutations affect biased dendrite growth perpendicular to GC axons. We focused on three mutations identified in earlier studies (Ikeda et al., 2006): L253P (a leucine to proline substitution in the calponin homology domain found in a German family); E532-M544 del (an in-frame 13 amino acid deletion in the third spectrin repeat found in an American family); and

L629-R634 delinsW (a five amino acid deletion with tryptophan insertion in the third spectrin repeat found in a French family) (Fig. 8A). The amino acid sequences related to these mutations are conserved among humans and mice. Thus, we generated mouse βIII spectrin mutant constructs harboring the corresponding mutations. These constructs were designed to be shRNA resistant and were tagged with a myc epitope at their N-termini for imaging.

Dissociated PCs on aligned nanofibers were knocked down for endogenous βIII spectrin and concomitantly transfected with wild-type βIII spectrin or disease-related mutants. Wild-type βIII spectrin was distributed in the somatodendritic area up to the most distal dendritic regions. In sharp contrast, the L253P form was localized in intracellular vesicular structures in the somatic area, whereas almost no signal was observed in dendrites (Fig. 8B). On the contrary, mutants with deletions in the third spectrin repeat (E532-M544 del and L629-R634 delinsW) localized to the dendritic plasma membrane to a lesser extent than the wild type. Quantitative image analysis revealed the differential localization of mutants in PC dendrites (Fig. 8C).

PCs expressing the shRNA-resistant wild-type molecule exhibited normal perpendicular dendrites. By contrast, all disease mutants were defective in the regulation of perpendicular dendrite formation. L253P and E532-M544 del were completely incompetent in perpendicular guidance, whereas the L629-R634 delinsW, which showed modest mislocalization, retained weak but significant guidance activity (Fig. 8D). Given that the disease mutants examined are associated with dominant forms of SCA5, we next asked whether the disease mutants act dominantly in the wild-type background without the knockdown plasmid. Although the effects were weak, these disease mutants affected the dendrite orientation (Fig. S9), supporting that these mutants mimic disease phenotypes.

To confirm the effect of the L253P and E532-M544 del mutations in the planar dendrite arborization *in vivo*, we delivered βIII spectrin-knockdown plasmid and shRNA resistant βIII spectrin wild type, L253P or E532-M544 del to immature PCs by *in utero* electroporation. Consistent with *in vitro* observation, L253P and E532-M544 del exhibited abnormal localization in vesicular structures in the soma and proximal dendritic surface, respectively, in contrast to the wild type spreading over the entire dendritic surface (Fig. 8E). PCs expressing the wild type showed planar dendrites, whereas cells expressing either L253P or E532-M544 del displayed disorganized dendrites growing away from the main dendritic plane (Fig. 8E,F). These results suggest that these disease mutations of βIII spectrin disrupt dendritic configuration in PCs.

DISCUSSION

In this study, we established a simplified 2D model of axon-dendrite topology using aligned nanofibers and confirmed that PC dendrites grew preferentially in the direction perpendicular to the bundles of afferent parallel fiber axons. Directional arborization is likely to be a prerequisite for the planar dendrite formation *in vivo*. Moreover, we revealed that biased dendrite arborization was affected by the loss of αII/βIII spectrins. In control PCs, dendritic branches were formed mainly by terminal bifurcation, with only a few collateral branches emerging from proximal dendrites (Fujishima et al., 2012). By contrast, lateral branching events were significantly increased in βIII spectrin-knockdown cells (Fig. 4G).

Dendritic protrusions in differentiating neurons serve as either branch precursors or immature spines (Heiman and Shaham, 2010; Yuste and Bonhoeffer, 2004). Dendrites of developing PCs in culture exhibited numerous lateral protrusions expressing the postsynaptic protein GluD2, suggesting that these lateral protrusions at the proximal dendrites are immature spine precursors. Notably, βIII spectrin-knockdown dendrites abnormally extended some proximal protrusions to a length indistinguishable from that of dendritic branches. These elongated protrusions bore multiple GluD2 puncta along their length, which interact with neurexins/Cbln1 expressed in GC axons. Thus, the loss of βIII spectrin seems to alter the fate of proximal dendritic protrusions from immature spines to misoriented lateral branches extending along the GC axons away from the main parasagittal plane.

Microtubule dynamics and dendritic branching

Branch formation requires microtubule extension into the precursor protrusions or filopodia, which is regulated by dynamic interplay with actin (Burnette et al., 2007; Flynn et al., 2012; Hu et al., 2012). It has been demonstrated that bundled actin in dendritic filopodia guides microtubules into filopodial protrusions from dendritic shafts, while the cortical actin meshwork in the shaft region confines microtubules and suppresses the interaction with bundled actin filaments in filopodia (Dent et al., 2007).

βIII spectrin was enriched in the thin neck regions of dendritic protrusions and the dendritic shaft and formed regular or irregular membrane skeletons (Fig. 6H; Fig. S7). We assume that βIII spectrin forms the membrane skeletons in coordination with cortical actin that functions as a molecular fence dividing the dendritic shaft and protrusions, confining microtubule dynamics along dendrites. Consistently, it has been shown that βIII spectrin regulates constricted neck formation in dendritic protrusions (Efimova et al., 2017). Thus, in βIII spectrin-deficient PCs, dendritic protrusions were often misshapen, with actin signals expanded to the protrusion base and dendritic shaft, in contrast to the confined localization in the tip of protrusions in normal cells (Fig. 6G,J). Mislocalized actin filaments and, possibly, actin-microtubule crosslinkers, such as Navigator1, Drebrin1 and p140Cap (Geraldo et al., 2008; Jaworski et al., 2009; van Haren et al., 2014), might interact with dynamic microtubules in the shaft and enhance their entry into the protrusion. Alternatively, it is also possible that some spectrin-binding proteins (4.1 proteins, ankyrins), which also interact with microtubules (Chen et al., 2020; Leterrier et al., 2011; Ruiz-Saenz et al., 2013), might contribute to the formation of a molecular fence at the protrusion base to block microtubule entry.

Although βIII spectrin distributes throughout the entire dendritic length, abnormal microtubule entry to protrusions was seen only in proximal dendrites in βIII spectrin-knockdown cells. We speculate that spectrin structures, including MPS structures, are gradually stabilized along the proximal to distal axis. In normal PCs, proximal dendritic shafts would already be covered by stable spectrin structures that impede microtubule invasion into protrusions, whereas the growing end of dendrites with immature spectrin structures allow microtubule entry that enhances dendrite extension. In βIII spectrin-knockdown cells, inhibition of microtubule entry into the proximal dendritic protrusions would be disrupted and thus induce abnormal lateral branching. Further studies are required to elucidate this hypothesis.

SCA5-related mutations affect dendrite growth in PCs

SCA5 is one of the autosomal dominant cerebellar ataxias caused by heterozygous mutation in the βIII spectrin gene (Ikeda et al., 2006). Although our experiment might not completely mimic the disease condition, some SCA5-related mutants misexpressed in βIII spectrin-knockdown cells failed to substitute for wild-type βIII spectrin to control the dendrite orientation (Fig. 8), and the mutants dominantly affected dendritic orientation in the wild-type background (Fig. S9).

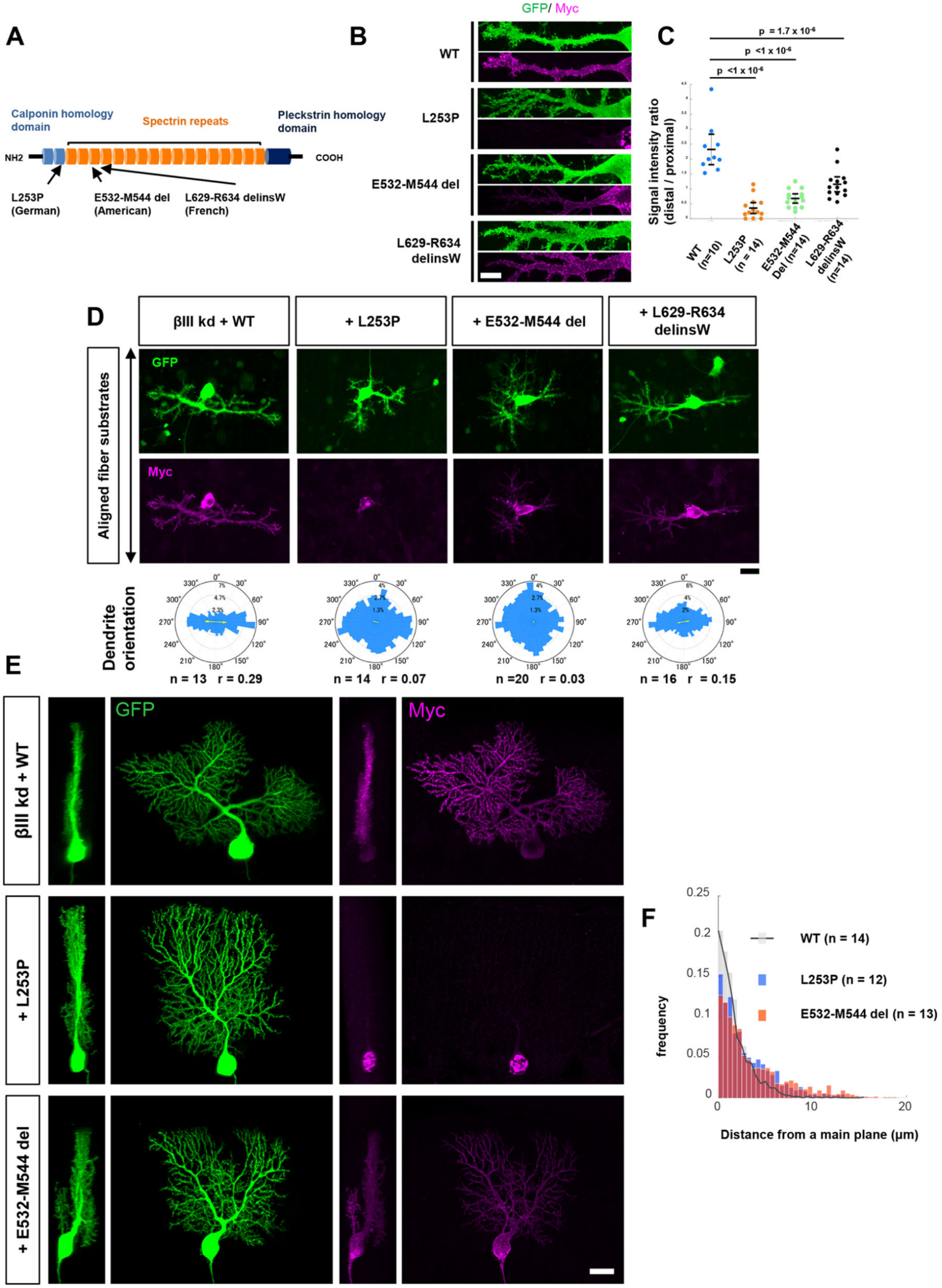

Fig. 8. Functional analysis of the effect of SCA5-related mutations on the regulation of dendrite orientation. (A) Domain structure of βIII spectrin and familial mutations associated with SCA5. (B) Localization of myc-tagged βIII spectrin wild type (WT), L253P, E532-M544 del or L629-R643 delinsW mutant in PCs (9 DIV). (C) Quantification of the signal intensity ratio (distal versus proximal) of βIII molecules in PC dendrites. Statistical analysis: Kruskal–Wallis test followed by Dunnett's test. (D) Morphologies of PCs transfected with GFP/shRNA-βIII spectrin plus βIII spectrin WT, L253P, E532-M544 del or L629-R643 delinsW grown on aligned nanofibers. Polar histograms indicate the angular distribution of dendritic segments. (E) Morphologies of PCs expressing the GFP/shRNA-βIII plasmid with βIII spectrin WT, L253P or E532-M544 del in P14 sagittal slices. (F) Proportions of dendritic segments locating at the indicated distances from the main plane. Scale bars: 10 μm in B; 20 μm in D,E.

L253P proteins were not delivered to dendritic membranes nor did they replace the function of the wild-type molecule in regulating the oriented dendrite growth. Consistently, previous studies have shown that the L253P mutation affects the trafficking of β-spectrin from the Golgi apparatus (Clarkson et al., 2010). It has also been suggested that the L253P mutation might reduce the plasticity of the actin-spectrin network by enhancing the actin-spectrin affinity. This change might affect the proper dendritic localization of βIII spectrin (Avery et al., 2017). By contrast, L629-R634 delinsW had only minor effects on dendritic localization and the oriented arborization of dendrites. Interestingly, E532-M544 del was severely defective in controlling dendrite growth orientation despite its relatively normal dendritic localization except for the distalmost region. It has been proposed that the deletion of E532-M544 possibly affects the triple α-helical structures of the spectrin repeats, which might result in the alteration of overall α/β structures (Ikeda et al., 2006). We assume that the E532-M544 del mutation might affect the stabilization of the spectrin architecture in dendrites and interfere with dendrite growth in the normal direction.

The SCA5 patients and βIII spectrin knockout animals exhibit progressive neurodegeneration that has been attributed to excitotoxicity owing to the mislocalization and the decreased level of glutamate transporters (Gao et al., 2011; Perkins et al., 2010, 2016b). Given that SCA5 is a late-onset cerebellar ataxia, it might be difficult to relate the developmentally disorganized dendrites observed in the present study directly to symptoms of the adult-onset disease. However, it is suggested that the thinner dendritic branches in the knockout PCs might alter signal propagation and contribute to the hyperexcitability (Gao et al., 2011). Abnormal branch growth in the coronal direction might lead to redundant and inefficient connectivity with parallel fibers (Cuntz, 2012). Furthermore, disruption of planarity is thought to affect the compartmentalization of cerebellar circuits. In the mature cerebellar cortex, each PC is innervated by a single climbing fiber axon of an inferior olive neuron. Coronally extended PC dendrites invading the neighboring PC territory might receive abnormal innervation by climbing fibers of neighboring PCs (Gao et al., 2011; Kaneko et al., 2011; Miyazaki and Watanabe, 2011; Perkins et al., 2016a). Developmental defects in dendrite arborization owing to the loss of βIII spectrin might deteriorate the cerebellar function before degeneration.

Remaining questions in the perpendicular axon-dendrite interactions

We demonstrate that PC dendrites grow perpendicular to parallel fibers, which seemingly contribute to the planar arborization *in vivo*. We also demonstrate that βIII spectrin is required for the perpendicular dendrite arborization by suppressing ectopic branch formation. However, considering that main dendritic frameworks still form planar patterns in the βIII spectrin-deficient PCs (Fig. 5B), βIII spectrin might function as a gatekeeper to maintain the perpendicular and planar dendrites but not as the main determinant regulating the directional dendrite extension.

The perpendicular interactions might serve as a permissive mechanism for the planar PC dendrite arborization in parasagittal planes. However, other mechanisms should also be involved in the spatial organization of dendrites, because perpendicular interactions would not assure arborization in the exact parasagittal plane. For instance, contact-based repulsion might support the flat dendrite formation by regulating the space between neighboring dendritic planes (Fig. 5A) (Fujishima et al., 2012; Ing-Esteves et al., 2018).

Nagata et al. (2006) previously proposed that the perpendicular interaction between PC dendrites and parallel fibers might be regulated by ‘contact guidance’, whereby cells recognize anisotropy of substrates to determine their directionality. Previous studies using carcinoma cells have demonstrated that anisotropic substrates affect the orientation of focal adhesions and actin fibers anchored to the adhesions, thereby leading to the directional movement (Ray et al., 2017). We assume that PC dendrites might sense the anisotropy of GC axons and adjust the orientation of adhesions and cytoskeletal components, including spectrin tetramers, thereby affecting the orientation of dendrite growth.

Previous studies using diffusion magnetic resonance imaging have revealed a three-dimensional grid-like organization of axonal bundles in the forebrain, in which two distinct fibers interweave and cross at nearly right angles (Wedeen et al., 2012). Such a grid-like organization might be formed by perpendicular contact between different types of axons. It is of interest to confirm whether perpendicular contact guidance is a general mechanism in neural network formation.

MATERIALS AND METHODS

Mice

Mice were handled in accordance with the guidelines of the Animal Experiment Committee of Kyoto University and were housed in a dedicated pathogen-free environment with a 12 h/12 h light/dark cycle.

Plasmids

The pAAV-CAG-GFP (or mCherry)-hH1 vector, including the human H1 promoter, was used to express shRNA to knockdown target gene expression, as previously described (Fukumitsu et al., 2015). The targeting sequences were designed by using the Web-based software siDirect (Naito et al., 2009): control shRNA (5′-GCATCTCCATTAGCGAACATT-3′), βIII spectrin shRNA (5′-GTCAATGTGCACAACTTTACC-3′) and αII spectrin shRNA (5′-GTAAAGACCTCACTAATGTCC-3′). To generate resistant mutants of αII spectrin and βIII spectrin that contained three silent mutations within shRNA target sequences, complementary DNA (cDNA) of mouse αII spectrin or βIII spectrin was cloned from a mouse brain cDNA library and mutagenized by using a PCR-based method. To generate the L253P, E532-M544 del and L629-R634 delinsW βIII spectrin mutants, PCR-based mutagenesis was performed by using the resistant mutant of βIII spectrin as a template. αII spectrin tagged with hemagglutinin (HA) at the N-terminus and βIII spectrin wild-type and mutant sequences tagged with myc at the N-terminus were cloned into the pCAGGS vector. To generate the EB3-EGFP construct, the coding sequence of EB3 was amplified from a mouse brain cDNA library and inserted into the pAAV-CAG-EGFP plasmid. For the CRISPR/Cas9-based knockout of βIII spectrin, the guide RNA sequence was selected by using the Web-based software CRISPRdirect (Naito et al., 2015). The βIII spectrin target sequence (5′-GAGACCTGTACAGCGACCTG-3′) was inserted into pSpCas9(BB)-2A-GFP (PX458) (Addgene plasmid #48138) (Ran et al., 2013).

In utero electroporation

The *in utero* electroporation of plasmids was performed as described previously (Nishiyama et al., 2012). Briefly, pregnant mice on day 11.5 of gestation were deeply anesthetized via the intra-abdominal injection of a mixture of medetomidine, midazolam and butorphanol. Plasmid DNA (1-5 μg/μl) was microinjected into the fourth ventricle of the embryos (FemtoJet; Eppendorf). Then, five current pulses (amplitude, 33 V; duration, 30 ms; intervals, 970 ms) were delivered with a forceps-shaped electrode (CUY650P3; NepaGene) connected to an electroporator (CUY21; NepaGene).

In vivo electroporation to label parallel fibers

The *in vivo* electroporation of plasmids was performed as described previously (Umeshima et al., 2007). P8 ICR mice were cryoanesthetized. A small burr hole was made in the skull over the cerebellum with a 27-gauge needle. The plasmid DNA (pAAV-CAG-mCherry) was microinjected through the hole by using a syringe with a 33-gauge needle (Ito). A forceps-shaped electrode connected to the cathode of an electroporator (CUY21; NepaGene) was placed in the occipital region. A needle used for DNA injection was connected to the anode. Then, six current pulses (amplitude, 70 V; duration, 50 ms; intervals, 150 ms) were delivered. After the wound was sutured, the pups were warmed at 37°C and returned to the home cage.

Primary cerebellar culture and nucleofection of cerebellar neurons

The primary culture of cerebellar neurons was performed as previously described (Fujishima et al., 2012) with slight modifications. Cerebella from P0 mice were dissected in Hank's balanced salt solution (Gibco) and dissociated using a Neuron Dissociation Kit (FUJIFILM Wako Pure Chemicals). Cells were plated on a 12 mm coverslip coated with poly-D-lysine in Dulbecco's modified Eagle's medium/Ham's F12 (DMEM/F12) supplemented with 10% fetal bovine serum at a density of 1.5 cerebella per coverslip. Following incubation, the media were replaced with maintenance media containing DMEM/F12, 0.1 mg/ml bovine serum albumin, 2.1 mg/ml glucose, 2× Glutamax, 8 µM progesterone, 20 µg/ml insulin, 200 µg/ml transferrin, 100 µM putrescine, 30 nM selenium dioxide, 4 µM AraC and 1% penicillin-streptomycin. For cultures on nanofibers, dissociated neurons were plated on aligned or random nanofiber plates (Nanofiber Solutions).

For the transfection of plasmid DNA into PCs, nucleofection was performed as described previously (Kawabata Galbraith et al., 2018). Briefly, dissociated cerebellar cells from between 1.5 and two cerebella were washed twice with OptiMEM and resuspended in 100 µl of OptiMEM containing 5-8 µg of plasmid DNA. Cells were transferred to a cuvette and nucleofected with a Nepa21 electroporator (NEPA GENE).

To separate the large cell fraction (containing PCs, interneurons and glia) and the small cell fraction (containing GCs), dissociated cells from P0 cerebellar tissue were purified with a step gradient of Percoll (Hatten, 1985). Isolated GCs from P0 mice were plated on the aligned fibers at a density of 10×10^5, 7×10^5 or 5×10^5 cells/cm^2. Then, the large cell fraction including PCs was plated on the culture at a density of 10×10^4, 7×10^4 or 5×10^4 cells/cm^2, respectively.

For the co-culture of cerebellar microexplants and PCs, a microexplant culture from cerebellar tissues was prepared as described previously (Nakatsuji and Nagata, 1989). Briefly, the external granular layer of the cerebellar cortex from P2 mice was dissected into 300-500 µm pieces and plated on the poly-D-lysine- and laminin-coated coverslips. One day after plating, the isolated large cell fraction including PCs from P0 mice was added to the culture.

Immunofluorescence and image acquisition

For immunocytochemistry, cells cultured on coverslips or nanofibers were fixed for 15 min at room temperature in 4% paraformaldehyde (PFA) in PBS. Cells were washed and permeabilized with PBS containing 0.25% Triton (PBS-0.25 T). The cells were then blocked with a blocking solution [PBS (−0.25 T) with 2% bovine serum albumin] for 30 min at room temperature. The cells were incubated with primary antibodies at 4°C overnight in the blocking solution, washed with PBS and incubated with fluorescently labeled secondary antibodies in blocking solution (for details of the antibodies used, see Table S1).

For immunohistochemistry, the mice were anesthetized with isoflurane and perfused with PBS followed by 4% PFA in phosphate buffer. Their brains were removed and postfixed overnight in 4% PFA/PBS at 4°C. After washing with PBS, the brains were embedded in a 3.5% low-melt agarose in PBS. Sagittal or coronal sections were cut at a thickness of 50-100 µm using a vibratome (Dosaka). The sections were permeabilized in PBS with 0.5% Triton (PBS-0.5 T) and blocked with 2% skim milk in PBS (−0.5 T) for 30 min. The sections were incubated with primary antibodies at 4°C overnight in blocking solution, washed with PBS and incubated with fluorescently labeled secondary antibodies in 2% skim milk in PBS (−0.5 T).

Images of the fixed samples were acquired on a laser scanning confocal microscope (Fluoview FV1000; Olympus) equipped with UPLSAPO 40× dry (NA 0.95), 60× water-immersion (NA 1.2) and 100× oil-immersion objectives (NA 1.40). For the imaging of PC dendrites in the cerebellar tissue, serial confocal *z*-stack images were acquired from midsagittal regions in lobes IV-V with the 60× objective at a *z*-step of 0.57 µm. The images were three-dimensionally reconstructed by using Imaris software (Bitplane). For the imaging of PC dendrites in the dissociated culture, serial confocal *z*-stack images were obtained with 40× or 100× objectives.

Quantification of dendrite morphology

For the analysis of dendritic flatness, captured confocal *z*-stacked images were binarized and skeletonized in ImageJ ['*Skeletonize* (*2D*/*3D*)' plugin]. To identify the plane with the closest fit to the given dendritic arbor, a principal components analysis was performed in MATLAB software (Fig. S2). To analyze the distance of the dendritic branches from the fitted plane, 3000 points (for Fig. 1A,B) or 100 points (for Fig. 1D; Fig. 3E; Fig. 8E) in the skeletonized dendritic images from each cell were randomly selected, and the distance between each point and the fitted plane was calculated.

For the morphometric analysis of PC dendrites on aligned fibers, *z*-projected images were binarized and skeletonized in the ImageJ plugin or MATLAB software. To analyze the branch angle, dendritic branches were divided into 3.5 µm segments, and the angle between each segment and fiber was quantified (Fig. S3).

STED imaging

We used a Leica TCS SP8 STED with an oil immersion 100× objective lens with NA 1.4 (HC-PL-APO 100×/1.4 OIL, Leica) to analyze the subcellular localization of βIII spectrin. The protein was labeled with anti-βIII spectrin (Santa Cruz, SC-28273, 1:100) and a secondary antibody conjugated with Alexa555 (Thermo Fisher A-31572, 1:1000). The fluorophore was excited with a white laser tuned to 555 nm and depleted with a 660 nm STED laser. A time gate window of 0.35-3.85 ns was used to maximize the STED resolution.

Time-lapse imaging, image processing and image analysis

For long-term time-lapse imaging, fluorescently labeled PCs were observed every 1-3 h with an incubation microscope (LCV100; Olympus) equipped with a 20× objective (NA 0.7; Olympus). Serial *z*-stacked images were obtained at *z*-steps of 1 µm (1 µm×five steps).

For the high-resolution live imaging of dendritic arbors (used for EB3 imaging experiments), for the analysis of EB3 dynamics, we used 10-11 DIV PC dendrites transfected with pAAV-CA-EB3-EGFP and pAAV-CAG-mCherry/hH1-control or hH1-βIII spectrin. Time-lapse images were obtained with a confocal microscope (FV1000, BX61W1; Olympus) equipped with a LUMFI 60× objective (NA 1.10; Olympus) under 5% CO_2 supplementation. Images were recorded with 3× digital zoom at an interval of 3 s. To eliminate background cytosolic signals, average subtraction was performed (Schätzle et al., 2016), in which an average projection of all the time-lapse images of EB3-EGFP signals was generated and subtracted from each frame of the time-lapse images. The images were then processed via an unsharp masking procedure in ImageJ software to obtain the enhanced images. For the quantitative analysis, the number of dendritic protrusions in the dendritic segments of 10 µm at the most distal regions or proximal regions (more than 10 µm away from the most distal end) were counted in ImageJ. Of those, dendritic protrusions invaded by the EB3-EGFP were identified manually with the assistance of the ImageJ plugin TrackMate (Tinevez et al., 2017).

Acknowledgements

We thank iCeMS Analysis Center and Dr Yukiko Ohara for technical assistance.

Competing interests

The authors declare no competing or financial interests.

Author contributions

Conceptualization: K.F., M.K.; Methodology: K.F., M.K.; Formal analysis: K.F., J.K., M.Y.; Investigation: K.F., J.K., M.Y.; Writing - original draft: K.F., M.K.; Writing - review & editing: K.F., M.K.

Funding

This work was supported by KAKENHI grants from the Japan Society for the Promotion of Science (16H06484 and 17K19453 to M.K., 16K18363 and 16KT0171 to K.F.) and Takeda Science Foundation to K.F.

Supplementary information

Supplementary information available online at
https://dev.biologists.org/lookup/doi/10.1242/dev.194530.supplemental

References

Albrecht, D., Winterflood, C. M., Sadeghi, M., Tschager, T., Noé, F. and Ewers, H. (2016). Nanoscopic compartmentalization of membrane protein motion at the axon initial segment. *J. Cell Biol.* **215**, 37-46. doi:10.1083/jcb.201603108

Altman, J. (1973). Experimental reorganization of the cerebellar cortex. IV. Parallel fiber reorientation following regeneration of the external germinal layer. *J. Comp. Neurol.* **149**, 181-191. doi:10.1002/cne.901490204

Altman, J. and Anderson, W. J. (1972). Experimental reorganization of the cerebellar cortex. I. Morphological effects of elimination of all microneurons with prolonged x-irradiation started at birth. *J. Comp. Neurol.* **146**, 355-405. doi:10.1002/cne.901460305

Armbrust, K. R., Wang, X., Hathorn, T. J., Cramer, S. W., Chen, G., Zu, T., Kangas, T., Zink, A. N., Öz, G., Ebner, T. J. et al. (2014). Mutant β-III spectrin causes mGluR1α mislocalization and functional deficits in a mouse model of spinocerebellar ataxia Type 5. *J. Neurosci.* **34**, 9891-9904. doi:10.1523/JNEUROSCI.0876-14.2014

Avery, A. W., Fealey, M. E., Wang, F., Orlova, A., Thompson, A. R., Thomas, D. D., Hays, T. S. and Egelman, E. H. (2017). Structural basis for high-affinity actin binding revealed by a β-III-spectrin SCA5 missense mutation. *Nat. Commun.* **8**, 1350. doi:10.1038/s41467-017-01367-w

Burnette, D. T., Schaefer, A. W., Ji, L., Danuser, G. and Forscher, P. (2007). Filopodial actin bundles are not necessary for microtubule advance into the peripheral domain of *Aplysia* neuronal growth cones. *Nat. Cell Biol.* **9**, 1360-1369. doi:10.1038/ncb1655

Chen, K., Yang, R., Li, Y., Zhou, J. C. and Zhang, M. (2020). Giant ankyrin-B suppresses stochastic collateral axon branching through direct interaction with microtubules. *J. Cell Biol.* **219**. doi:10.1083/jcb.201910053

Cianci, C. D., Zhang, Z., Pradhan, D. and Morrow, J. S. (1999). Brain and muscle express a unique alternative transcript of αII spectrin. *Biochemistry* **38**, 15721-15730. doi:10.1021/bi991458k

Clarkson, Y. L., Gillespie, T., Perkins, E. M., Lyndon, A. R. and Jackson, M. (2010). β-III spectrin mutation L253P associated with spinocerebellar ataxia type 5 interferes with binding to Arp1 and protein trafficking from the Golgi. *Hum. Mol. Genet.* **19**, 3634-3641. doi:10.1093/hmg/ddq279

Crepel, F., Delhaye-Bouchaud, N., Dupont, J. L. and Sotelo, C. (1980). Dendritic and axonic fields of purkinje cells in developing and X-irradiated rat cerebellum. a comparative study using intracellular staining with horseradish peroxidase. *Neuroscience* **5**, 333-347. doi:10.1016/0306-4522(80)90109-8

Cuntz, H. (2012). The dendritic density field of a cortical pyramidal cell. *Front. Neuroanat.* **6**, 2. doi:10.3389/fnana.2012.00002

Dent, E. W., Kwiatkowski, A. V., Mebane, L. M., Philippar, U., Barzik, M., Rubinson, D. A., Gupton, S., Van Veen, J. E., Furman, C., Zhang, J. et al. (2007). Filopodia are required for cortical neurite initiation. *Nat. Cell Biol.* **9**, 1347-1359. doi:10.1038/ncb1654

D'Este, E., Kamin, D., Göttfert, F., El-Hady, A. and Hell, S. W. (2015). STED nanoscopy reveals the ubiquity of subcortical cytoskeleton periodicity in living neurons. *Cell Rep.* **10**, 1246-1251. doi:10.1016/j.celrep.2015.02.007

Dong, X., Shen, K. and Bülow, H. E. (2015). Intrinsic and extrinsic mechanisms of dendritic morphogenesis. *Annu. Rev. Physiol.* **77**, 271-300. doi:10.1146/annurev-physiol-021014-071746

Efimova, N., Korobova, F., Stankewich, M. C., Moberly, A. H., Stolz, D. B., Wang, J., Kashina, A., Ma, M. and Svitkina, T. (2017). βIII spectrin is necessary for formation of the constricted neck of dendritic spines and regulation of synaptic activity in neurons. *J. Neurosci.* **37**, 6442-6459. doi:10.1523/JNEUROSCI.3520-16.2017

Engelkamp, D., Rashbass, P., Seawright, A. and van Heyningen, V. (1999). Role of Pax6 in development of the cerebellar system. *Development* **126**, 3585-3596.

Flynn, K. C., Hellal, F., Neukirchen, D., Jacob, S., Tahirovic, S., Dupraz, S., Stern, S., Garvalov, B. K., Gurniak, C., Shaw, A. E. et al. (2012). ADF/cofilin-mediated actin retrograde flow directs neurite formation in the developing brain. *Neuron* **76**, 1091-1107. doi:10.1016/j.neuron.2012.09.038

Fujishima, K., Horie, R., Mochizuki, A. and Kengaku, M. (2012). Principles of branch dynamics governing shape characteristics of cerebellar Purkinje cell dendrites. *Development* **139**, 3442-3455. doi:10.1242/dev.081315

Fujishima, K., Kawabata Galbraith, K. and Kengaku, M. (2018). Dendritic self-avoidance and morphological development of cerebellar Purkinje cells. *Cerebellum* **17**, 701-708. doi:10.1007/s12311-018-0984-8

Fukumitsu, K., Fujishima, K., Yoshimura, A., Wu, Y. K., Heuser, J. and Kengaku, M. (2015). Synergistic action of dendritic mitochondria and creatine kinase maintains ATP homeostasis and actin dynamics in growing neuronal dendrites. *J. Neurosci.* **35**, 5707-5723. doi:10.1523/JNEUROSCI.4115-14.2015

Gao, Y., Perkins, E. M., Clarkson, Y. L., Tobia, S., Lyndon, A. R., Jackson, M. and Rothstein, J. D. (2011). β-III spectrin is critical for development of Purkinje cell dendritic tree and spine morphogenesis. *J. Neurosci.* **31**, 16581-16590. doi:10.1523/JNEUROSCI.3332-11.2011

Geraldo, S., Khanzada, U. K., Parsons, M., Chilton, J. K. and Gordon-Weeks, P. R. (2008). Targeting of the F-actin-binding protein drebrin by the microtubule plus-tip protein EB3 is required for neuritogenesis. *Nat. Cell Biol.* **10**, 1181-1189. doi:10.1038/ncb1778

Gibson, D. A., Tymanskyj, S., Yuan, R. C., Leung, H. C., Lefebvre, J. L., Sanes, J. R., Chédotal, A. and Ma, L. (2014). Dendrite self-avoidance requires cell-autonomous slit/robo signaling in cerebellar Purkinje cells. *Neuron* **81**, 1040-1056. doi:10.1016/j.neuron.2014.01.009

Han, C., Wang, D., Soba, P., Zhu, S., Lin, X., Jan, L. Y. and Jan, Y.-N. (2012). Integrins regulate repulsion-mediated dendritic patterning of Drosophila sensory neurons by restricting dendrites in a 2D space. *Neuron* **73**, 64-78. doi:10.1016/j.neuron.2011.10.036

Han, B., Zhou, R., Xia, C. and Zhuang, X. (2017). Structural organization of the actin-spectrin–based membrane skeleton in dendrites and soma of neurons. *Proc. Natl. Acad. Sci. USA* **114**, E6678-E6685. doi:10.1073/pnas.1705043114

Hatten, M. E. (1985). Neuronal regulation of astroglial morphology and proliferation in vitro. *J. Cell Biol.* **100**, 384-396. doi:10.1083/jcb.100.2.384

Heiman, M. G. and Shaham, S. (2010). Twigs into branches: how a filopodium becomes a dendrite. *Curr. Opin. Neurobiol.* **20**, 86-91. doi:10.1016/j.conb.2009.10.016

Hu, J., Bai, X., Bowen, J. R., Dolat, L., Korobova, F., Yu, W., Baas, P. W., Svitkina, T., Gallo, G. and Spiliotis, E. T. (2012). Septin-driven coordination of actin and microtubule remodeling regulates the collateral branching of axons. *Curr. Biol.* **22**, 1109-1115. doi:10.1016/j.cub.2012.04.019

Hyysalo, A., Ristola, M., Joki, T., Honkanen, M., Vippola, M. and Narkilahti, S. (2017). Aligned Poly(ε-caprolactone) nanofibers guide the orientation and migration of human pluripotent stem cell-derived neurons, astrocytes, and oligodendrocyte precursor cells in vitro. *Macromol. Biosci.* **17**, 1600517. doi:10.1002/mabi.201600517

Ikeda, Y., Dick, K. A., Weatherspoon, M. R., Gincel, D., Armbrust, K. R., Dalton, J. C., Stevanin, G., Dürr, A., Zühlke, C., Bürk, K. et al. (2006). Spectrin mutations cause spinocerebellar ataxia type 5. *Nat. Genet.* **38**, 184-190. doi:10.1038/ng1728

Ing-Esteves, S., Kostadinov, D., Marocha, J., Sing, A. D., Joseph, K. S., Laboulaye, M., Sanes, J. R. and Lefebvre, J. L. (2018). Combinatorial effects of Alpha- and Gamma-Protocadherins on neuronal survival and dendritic self-avoidance. *J. Neurosci.* **38**, 2713-2729. doi:10.1523/JNEUROSCI.3035-17.2018

Jan, Y.-N. and Jan, L. Y. (2010). Branching out: mechanisms of dendritic arborization. *Nat. Rev. Neurosci.* **11**, 316-328. doi:10.1038/nrn2836

Jaworski, J., Kapitein, L. C., Gouveia, S. M., Dortland, B. R., Wulf, P. S., Grigoriev, I., Camera, P., Spangler, S. A., Di Stefano, P., Demmers, J. et al. (2009). Dynamic microtubules regulate dendritic spine morphology and synaptic plasticity. *Neuron* **61**, 85-100. doi:10.1016/j.neuron.2008.11.013

Joo, W., Hippenmeyer, S. and Luo, L. (2014). Dendrite morphogenesis depends on relative levels of NT-3/TrkC signaling. *Science* **346**, 626-629. doi:10.1126/science.1258996

Kaneko, M., Yamaguchi, K., Eiraku, M., Sato, M., Takata, N., Kiyohara, Y., Mishina, M., Hirase, H., Hashikawa, T. and Kengaku, M. (2011). Remodeling of monoplanar Purkinje cell dendrites during cerebellar circuit formation. *PLoS ONE* **6**, e20108. doi:10.1371/journal.pone.0020108

Kapfhammer, J. P. (2004). Cellular and molecular control of dendritic growth and development of cerebellar Purkinje cells. *Prog. Histochem. Cytochem.* **39**, 131-182. doi:10.1016/j.proghi.2004.07.002

Kawabata Galbraith, K., Fujishima, K., Mizuno, H., Lee, S.-J., Uemura, T., Sakimura, K., Mishina, M., Watanabe, N. and Kengaku, M. (2018). MTSS1 regulation of actin-nucleating formin DAAM1 in dendritic filopodia determines final dendritic configuration of Purkinje cells. *Cell Rep.* **24**, 95-106.e9. doi:10.1016/j.celrep.2018.06.013

Kawaji, K., Umeshima, H., Eiraku, M., Hirano, T. and Kengaku, M. (2004). Dual phases of migration of cerebellar granule cells guided by axonal and dendritic leading processes. *Mol. Cell. Neurosci.* **25**, 228-240. doi:10.1016/j.mcn.2003.10.006

Kim, M. E., Shrestha, B. R., Blazeski, R., Mason, C. A. and Grueber, W. B. (2012). Integrins establish dendrite-substrate relationships that promote dendritic self-avoidance and patterning in Drosophila sensory neurons. *Neuron* **73**, 79-91. doi:10.1016/j.neuron.2011.10.033

Kim, J., Park, T.-J., Kwon, N., Lee, D., Kim, S., Kohmura, Y., Ishikawa, T., Kim, K.-T., Curran, T. and Je, J. H. (2014). Dendritic planarity of Purkinje cells is independent of Reelin signaling. *Brain Struct. Funct.* **220**, 2263-2273. doi:10.1007/s00429-014-0780-2

Krieg, M., Stühmer, J., Cueva, J. G., Fetter, R., Spilker, K., Cremers, D., Shen, K., Dunn, A. R. and Goodman, M. B. (2017). Genetic defects in β-spectrin and tau sensitize C. elegans axons to movement-induced damage via torque-tension coupling. *eLife* **6**, e20172. doi:10.7554/eLife.20172

Kuwako, K. and Okano, H. (2018). The LKB1-SIK pathway controls dendrite self-avoidance in purkinje cells. *Cell Rep.* **24**, 2808-2818.e4. doi:10.1016/j.celrep.2018.08.029

Lefebvre, J. L., Kostadinov, D., Chen, W. V., Maniatis, T. and Sanes, J. R. (2012). Protocadherins mediate dendritic self-avoidance in the mammalian nervous system. *Nature* **488**, 517-521. doi:10.1038/nature11305

Leite, S. C., Sampaio, P., Sousa, V. F., Nogueira-Rodrigues, J., Pinto-Costa, R., Peters, L. L., Brites, P. and Sousa, M. M. (2016). The Actin-Binding Protein α-Adducin Is Required for Maintaining Axon Diameter. *Cell Rep.* **15**, 490-498. doi:10.1016/j.celrep.2016.03.047

Leterrier, C., Vacher, H., Fache, M.-P., d'Ortoli, S. A., Castets, F., Autillo-Touati, A. and Dargent, B. (2011). End-binding proteins EB3 and EB1 link microtubules to ankyrin G in the axon initial segment. *Proc. Natl. Acad. Sci. USA* **108**, 8826-8831. doi:10.1073/pnas.1018671108

London, M. and Häusser, M. (2005). Dendritic computation. *Annu. Rev. Neurosci.* **28**, 503-532. doi:10.1146/annurev.neuro.28.061604.135703

Matsuda, K., Miura, E., Miyazaki, T., Kakegawa, W., Emi, K., Narumi, S., Fukazawa, Y., Ito-Ishida, A., Kondo, T., Shigemoto, R. et al. (2010). Cbln1 is a ligand for an orphan glutamate receptor δ2, a bidirectional synapse organizer. *Science* **328**, 363-368. doi:10.1126/science.1185152

Miyazaki, T. and Watanabe, M. (2011). Development of an anatomical technique for visualizing the mode of climbing fiber innervation in Purkinje cells and its application to mutant mice lacking GluRδ2 and Ca(v)2.1. *Anat. Sci. Int.* **86**, 10-18. doi:10.1007/s12565-010-0095-1

Nagata, I. and Nakatsuji, N. (1990). Granule cell behavior on laminin in cerebellar microexplant cultures. *Dev. Brain Res.* **52**, 63-73. doi:10.1016/0165-3806(90)90222-K

Nagata, I., Ono, K., Kawana, A. and Kimura-Kuroda, J. (2006). Aligned neurite bundles of granule cells regulate orientation of Purkinje cell dendrites by perpendicular contact guidance in two–dimensional and three–dimensional mouse cerebellar cultures. *J. Comp. Neurol.* **499**, 274-289. doi:10.1002/cne.21102

Naito, Y., Yoshimura, J., Morishita, S. and Ui-Tei, K. (2009). siDirect 2.0: updated software for designing functional siRNA with reduced seed-dependent off-target effect. *BMC Bioinformatics* **10**, 392. doi:10.1186/1471-2105-10-392

Naito, Y., Hino, K., Bono, H. and Ui-Tei, K. (2015). CRISPRdirect: software for designing CRISPR/Cas guide RNA with reduced off-target sites. *Bioinformatics* **31**, 1120-1123. doi:10.1093/bioinformatics/btu743

Nakatsuji, N. and Nagata, I. (1989). Paradoxical perpendicular contact guidance displayed by mouse cerebellar granule cell neurons in vitro. *Development* **106**, 441-447. doi:10.1016/0922-3371(89)90604-7

Napper, R. M. A. and Harvey, R. J. (1988). Number of parallel fiber synapses on an individual Purkinje cell in the cerebellum of the rat. *J. Comp. Neurol.* **274**, 168-177. doi:10.1002/cne.902740204

Nishiyama, J., Hayashi, Y., Nomura, T., Miura, E., Kakegawa, W. and Yuzaki, M. (2012). Selective and regulated gene expression in murine Purkinje cells by in utero electroporation. *Eur. J. Neurosci.* **36**, 2867-2876. doi:10.1111/j.1460-9568.2012.08203.x

Perkins, E. M., Clarkson, Y. L., Sabatier, N., Longhurst, D. M., Millward, C. P., Jack, J., Toraiwa, J., Watanabe, M., Rothstein, J. D., Lyndon, A. R. et al. (2010). Loss of β-III spectrin leads to purkinje cell dysfunction recapitulating the behavior and neuropathology of spinocerebellar ataxia type 5 in humans. *J. Neurosci.* **30**, 4857-4867. doi:10.1523/JNEUROSCI.6065-09.2010

Perkins, E., Suminaite, D. and Jackson, M. (2016a). Cerebellar ataxias: β-III spectrin's interactions suggest common pathogenic pathways. *J. Physiol.* **594**, 4661-4676. doi:10.1113/JP271195

Perkins, E. M., Suminaite, D., Clarkson, Y. L., Lee, S. K., Lyndon, A. R., Rothstein, J. D., Wyllie, D. J. A., Tanaka, K. and Jackson, M. (2016b). Posterior cerebellar Purkinje cells in an SCA5/SPARCA1 mouse model are especially vulnerable to the synergistic effect of loss of β-III spectrin and GLAST. *Hum. Mol. Genet.* **25**, 4448-4461. doi:10.1093/hmg/ddw274

Ran, F. A., Hsu, P. D., Wright, J., Agarwala, V., Scott, D. A. and Zhang, F. (2013). Genome engineering using the CRISPR-Cas9 system. *Nat. Protoc.* **8**, 2281-2308. doi:10.1038/nprot.2013.143

Ray, A., Lee, O., Win, Z., Edwards, R. M., Alford, P. W., Kim, D.-H. and Provenzano, P. P. (2017). Anisotropic forces from spatially constrained focal adhesions mediate contact guidance directed cell migration. *Nat. Commun.* **8**, 14923. doi:10.1038/ncomms14923

Ruiz-Saenz, A., van Haren, J., Sayas, C. L., Rangel, L., Demmers, J., Millán, J., Alonso, M. A., Galjart, N. and Correas, I. (2013). Protein 4.1R binds to CLASP2 and regulates dynamics, organization and attachment of microtubules to the cell cortex. *J. Cell Sci.* **126**, 4589-4601. doi:10.1242/jcs.120840

Schätzle, P., Kapitein, L. C. and Hoogenraad, C. C. (2016). Chapter 4 - Live imaging of microtubule dynamics in organotypic hippocampal slice cultures. In *Methods in Cell Biology* (ed. K. K. Pfister), pp. 107-126. Academic Press.

Shimada, A., Mason, C. A. and Morrison, M. E. (1998). TrkB signaling modulates spine density and morphology independent of dendrite structure in cultured neonatal Purkinje cells. *J. Neurosci.* **18**, 8559-8570. doi:10.1523/JNEUROSCI.18-21-08559.1998

Sotelo, C. and Dusart, I. (2009). Intrinsic versus extrinsic determinants during the development of Purkinje cell dendrites. *Neuroscience* **162**, 589-600. doi:10.1016/j.neuroscience.2008.12.035

Stankewich, M. C., Gwynn, B., Ardito, T., Ji, L., Kim, J., Robledo, R. F., Lux, S. E., Peters, L. L. and Morrow, J. S. (2010). Targeted deletion of βIII spectrin impairs synaptogenesis and generates ataxic and seizure phenotypes. *Proc. Natl. Acad. Sci. USA* **107**, 6022-6027. doi:10.1073/pnas.1001522107

Stankewich, M. C., Cianci, C. D., Stabach, P. R., Ji, L., Nath, A. and Morrow, J. S. (2011). Cell organization, growth, and neural and cardiac development require αII-spectrin. *J. Cell Sci.* **124**, 3956-3966. doi:10.1242/jcs.080374

Takeo, Y. H., Kakegawa, W., Miura, E. and Yuzaki, M. (2015). RORα regulates multiple aspects of dendrite development in cerebellar Purkinje cells In vivo. *J. Neurosci.* **35**, 12518-12534. doi:10.1523/JNEUROSCI.0075-15.2015

Tanaka, M. (2009). Dendrite formation of cerebellar Purkinje cells. *Neurochem. Res.* **34**, 2078-2088. doi:10.1007/s11064-009-0073-y

Tinevez, J.-Y., Perry, N., Schindelin, J., Hoopes, G. M., Reynolds, G. D., Laplantine, E., Bednarek, S. Y., Shorte, S. L. and Eliceiri, K. W. (2017). TrackMate: an open and extensible platform for single-particle tracking. *Methods* **115**, 80-90. doi:10.1016/j.ymeth.2016.09.016

Toyoda, S., Kawaguchi, M., Kobayashi, T., Tarusawa, E., Toyama, T., Okano, M., Oda, M., Nakauchi, H., Yoshimura, Y., Sanbo, M. et al. (2014). Developmental epigenetic modification regulates stochastic expression of clustered protocadherin genes, generating single neuron diversity. *Neuron* **82**, 94-108. doi:10.1016/j.neuron.2014.02.005

Uemura, T., Lee, S.-J., Yasumura, M., Takeuchi, T., Yoshida, T., Ra, M., Taguchi, R., Sakimura, K. and Mishina, M. (2010). Trans-synaptic interaction of GluRδ2 and neurexin through Cbln1 mediates synapse formation in the cerebellum. *Cell* **141**, 1068-1079. doi:10.1016/j.cell.2010.04.035

Umeshima, H., Hirano, T. and Kengaku, M. (2007). Microtubule-based nuclear movement occurs independently of centrosome positioning in migrating neurons. *Proc. Natl. Acad. Sci. USA* **104**, 16182-16187. doi:10.1073/pnas.0708047104

Valnegri, P., Puram, S. V. and Bonni, A. (2015). Regulation of dendrite morphogenesis by extrinsic cues. *Trends Neurosci.* **38**, 439-447. doi:10.1016/j.tins.2015.05.003

van Haren, J., Boudeau, J., Schmidt, S., Basu, S., Liu, Z., Lammers, D., Demmers, J., Benhari, J., Grosveld, F., Debant, A. et al. (2014). Dynamic microtubules catalyze formation of navigator-TRIO complexes to regulate neurite extension. *Curr. Biol.* **24**, 1778-1785. doi:10.1016/j.cub.2014.06.037

Vassilopoulos, S., Gibaud, S., Jimenez, A., Caillol, G. and Leterrier, C. (2019). Ultrastructure of the axonal periodic scaffold reveals a braid-like organization of actin rings. *Nat. Commun.* **10**, 5803. doi:10.1038/s41467-019-13835-6

Wedeen, V. J., Rosene, D. L., Wang, R., Dai, G., Mortazavi, F., Hagmann, P., Kaas, J. H. and Tseng, W.-Y. I. (2012). The geometric structure of the brain fiber pathways. *Science* **335**, 1628-1634. doi:10.1126/science.1215280

Wen, Q. and Chklovskii, D. B. (2008). A cost-benefit analysis of neuronal morphology. *J. Neurophysiol.* **99**, 2320-2328. doi:10.1152/jn.00280.2007

Winkelmann, J. C. and Forget, B. G. (1993). Erythroid and nonerythroid spectrins. *Blood* **81**, 3173-3185. doi:10.1182/blood.V81.12.3173.3173

Xu, K., Zhong, G. and Zhuang, X. (2013). Actin, spectrin, and associated proteins form a periodic cytoskeletal structure in axons. *Science* **339**, 452-456. doi:10.1126/science.1232251

Yuste, R. and Bonhoeffer, T. (2004). Genesis of dendritic spines: insights from ultrastructural and imaging studies. *Nat. Rev. Neurosci.* **5**, 24-34. doi:10.1038/nrn1300

Figure S1

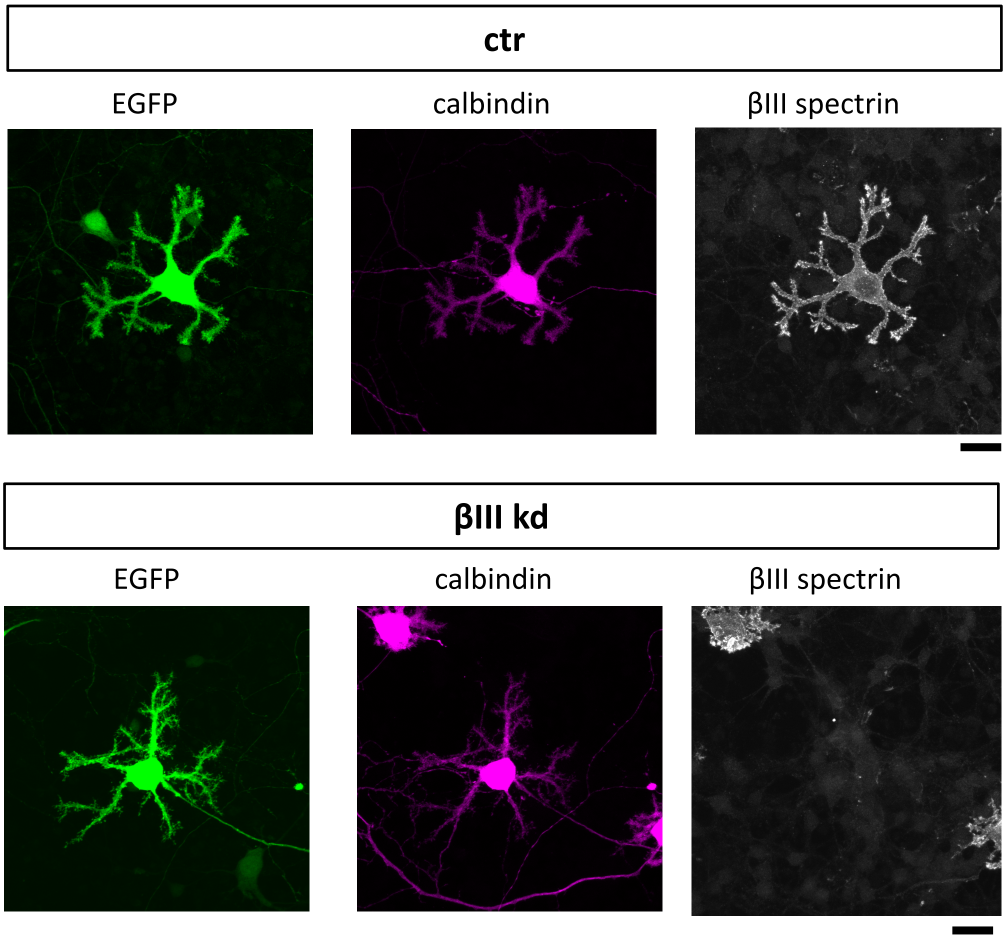

Fig. S1 Validation of shRNA targeting βIII spectrin in dissociation culture

Representative images of cerebellar PCs transfected with a plasmid containing EGFP/shRNA control (ctr) or EGFP/shRNA βIII spectrin (βIII kd). Cells were stained with anti-calbindin (magenta) and anti-βIII spectrin (white) antibodies. The calbindin-positive PCs transfected with the βIII knockdown plasmid lacked βIII spectrin signals. Scale bars: 20 µm.

Figure S2

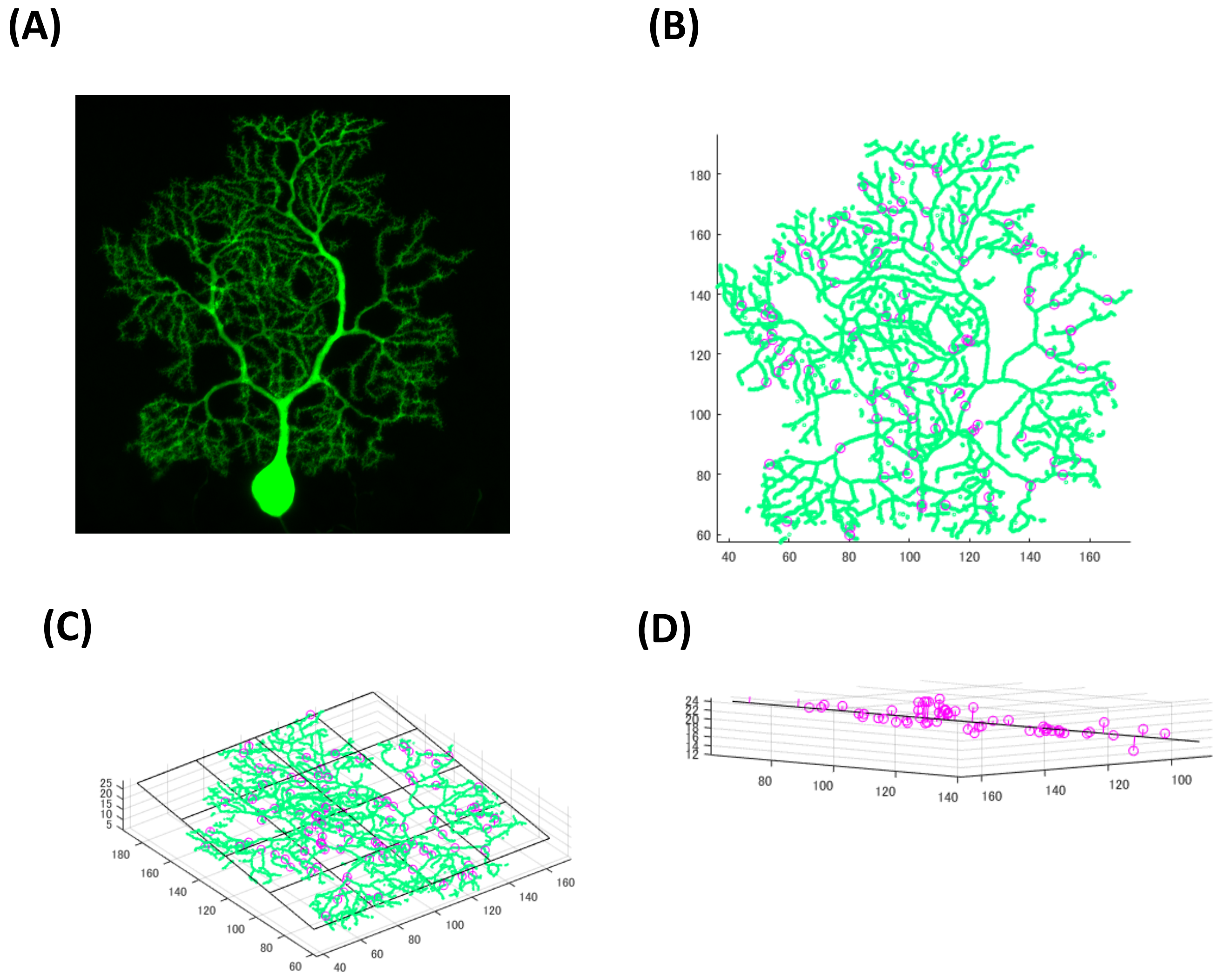

Fig. S2 Quantitative analysis of the planarity of PC dendrites in cerebellar tissue

(A) Representative image of cerebellar PCs labeled with GFP in a sagittal cerebellar slice at P14. **(B)** Skeletonized image of the PC dendrites in (A). Magenta points were randomly selected from the skeletonized dendrite. **(C)** A three-dimensional view of the skeletonized dendrite, randomly selected points, and a plane fitted to the dendrites. **(D)** A side view of randomly selected points and the dendritic plane.

Figure S3

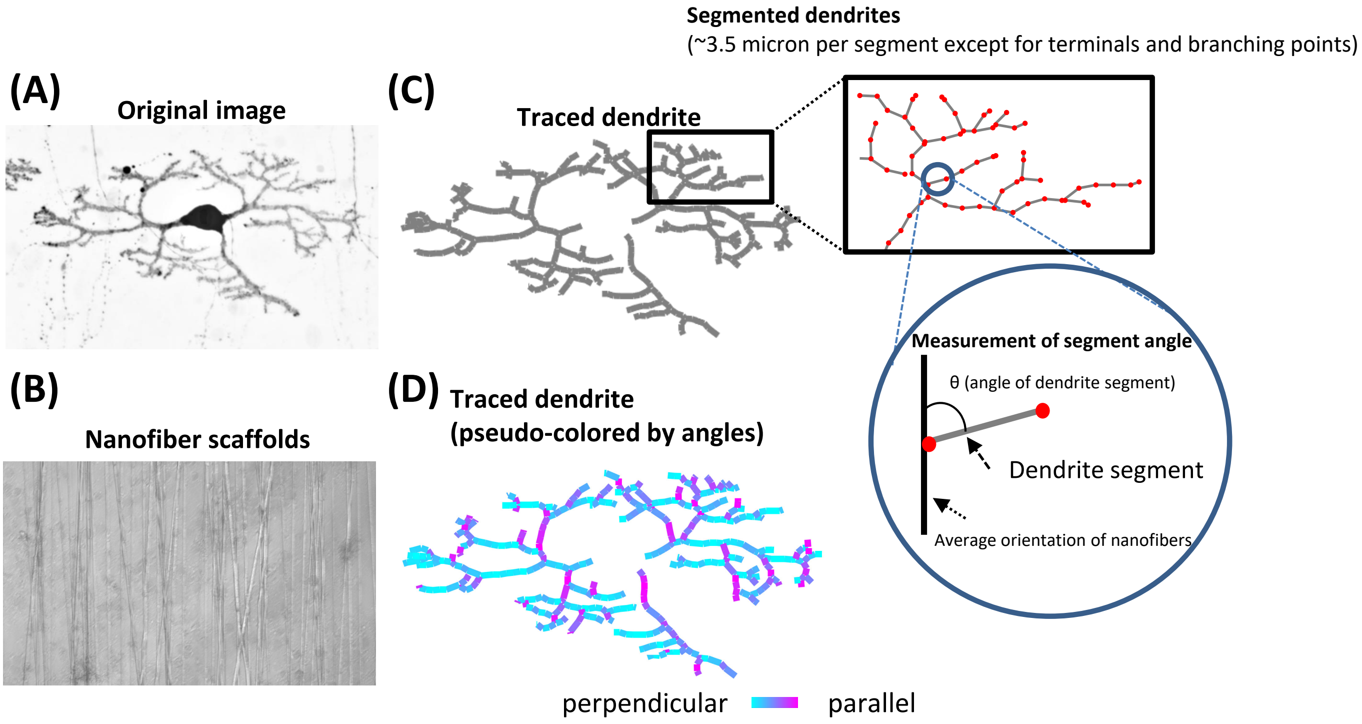

Fig. S3 Quantitative analysis of dendrite orientation in the culture using nanofiber substrates

(A) Representative image of PCs growing on the aligned nanofiber substrates. (B) A DIC image showing nanofibers. (C) Traced dendrites were divided into 3.5-micron segments. The angles of dendritic segments with respect to the average orientation of nanofibers were recorded. (D) The traced dendrites were pseudocolored by the orientation of the dendritic segments.

Figure S4

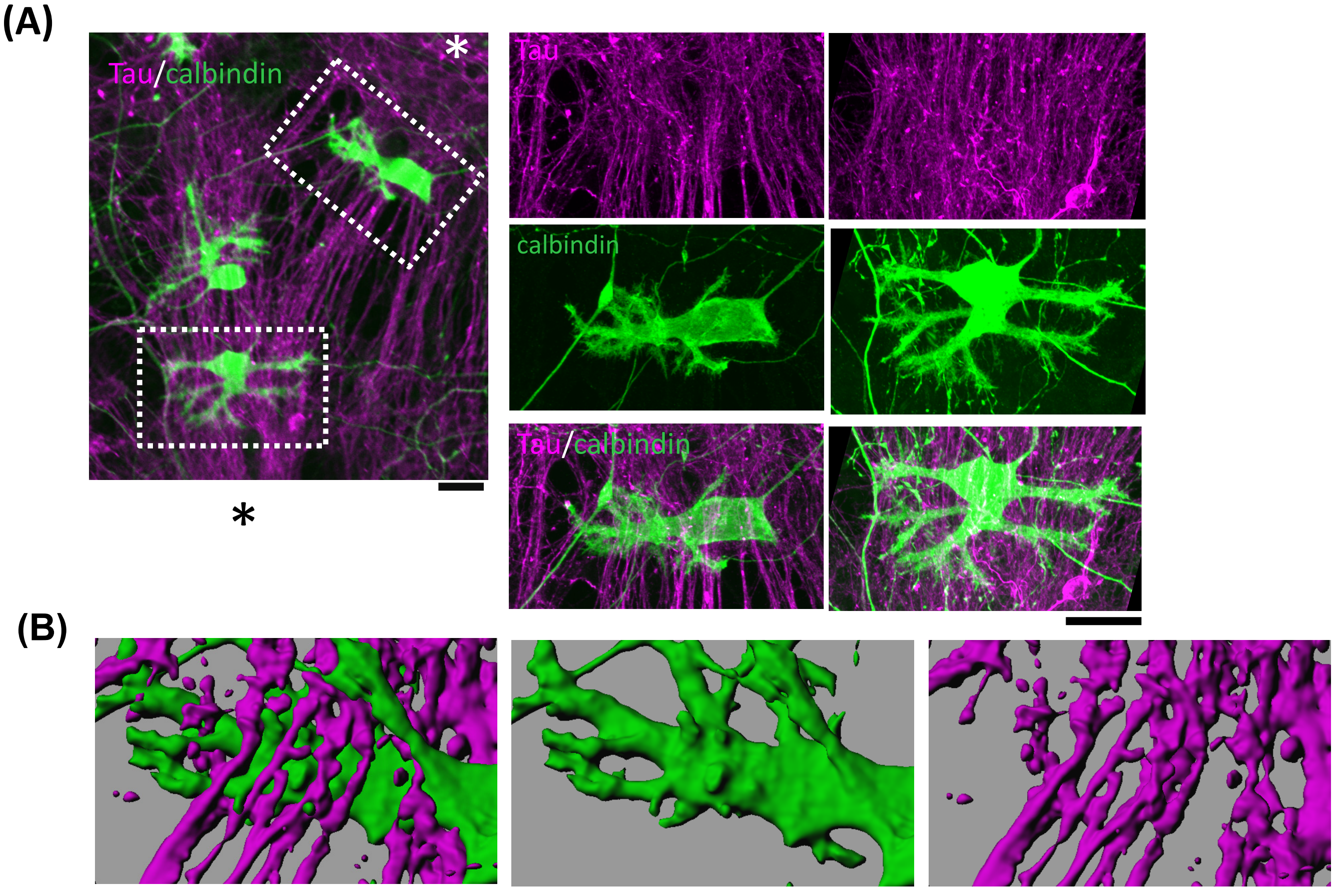

Fig. S4 Purkinje cell dendrites grow perpendicular to granule cell axons but not nanofibers

(A) Representative images of PCs (calbindin) grown on microexplant culture. Asterisks indicate the locations of microexplants. GCs extend their axons radially from the explants (tau). One day after the preparation of microexplants, large cells including PCs were isolated from cerebellar tissue by the Percoll gradient methods and plated on the explant. Microexplants and PCs were fixed at 9 days after the preparation of microexplants. Right panels were magnified views of the boxed region in the right image. (B) Surface rendering images showing the PC and GC axons.

Figure S5

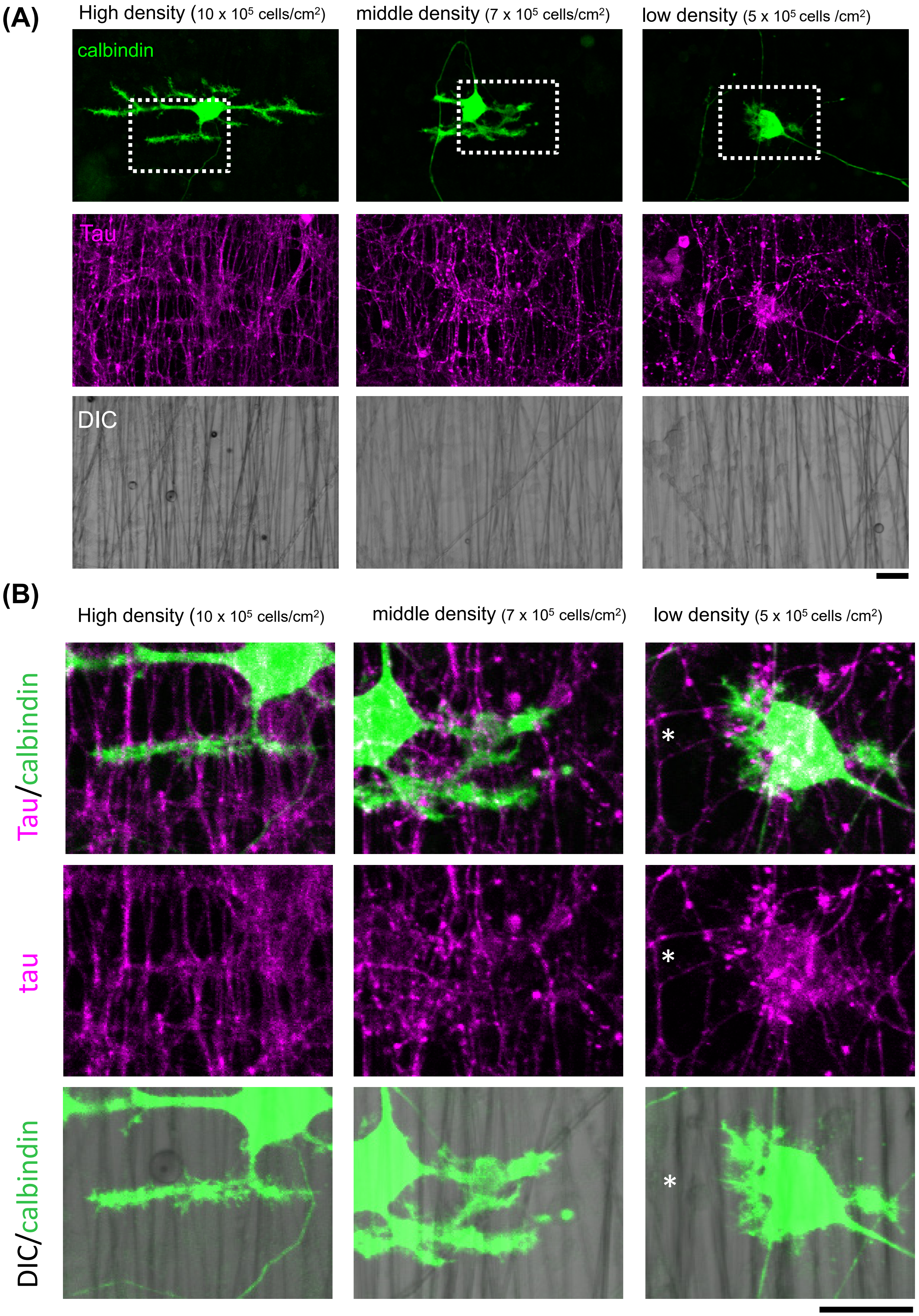
(A)
High density (10 x 10^5 cells/cm^2)
middle density (7 x 10^5 cells/cm^2)
low density (5 x 10^5 cells /cm^2)
calbindin
Tau
DIC
(B)
High density (10 x 10^5 cells/cm^2)
middle density (7 x 10^5 cells/cm^2)
low density (5 x 10^5 cells /cm^2)
Tau/calbindin
tau
DIC/calbindin
*
*
*

Fig. S5 Growth of Purkinje cell dendrites on the axonal fibers with different densities

(A) Representative images of PCs (calbindin) and GC axons (tau) grown on nanofiber substrates. GCs isolated by the Percoll gradient method were plated on the aligned nanofiber substrates at the density of 10 x 10^5/cm^2, 7 x 10^5/cm^2, or 5 x 10^5/cm^2. Large cells including PCs were plated at the density of 10 x 10^4/cm^2, 7 x 10^4/cm^2, or 5 x 10^4/cm^2, respectively. (B) Magnified views of dendrites in the boxed regions in (A). Note that PCs cannot extend their dendrite in the region where the density of GC axons is low, even though the region contains a comparable level of nanofiber substrates (asterisk). Scale bars: 20 µm.

Figure S6

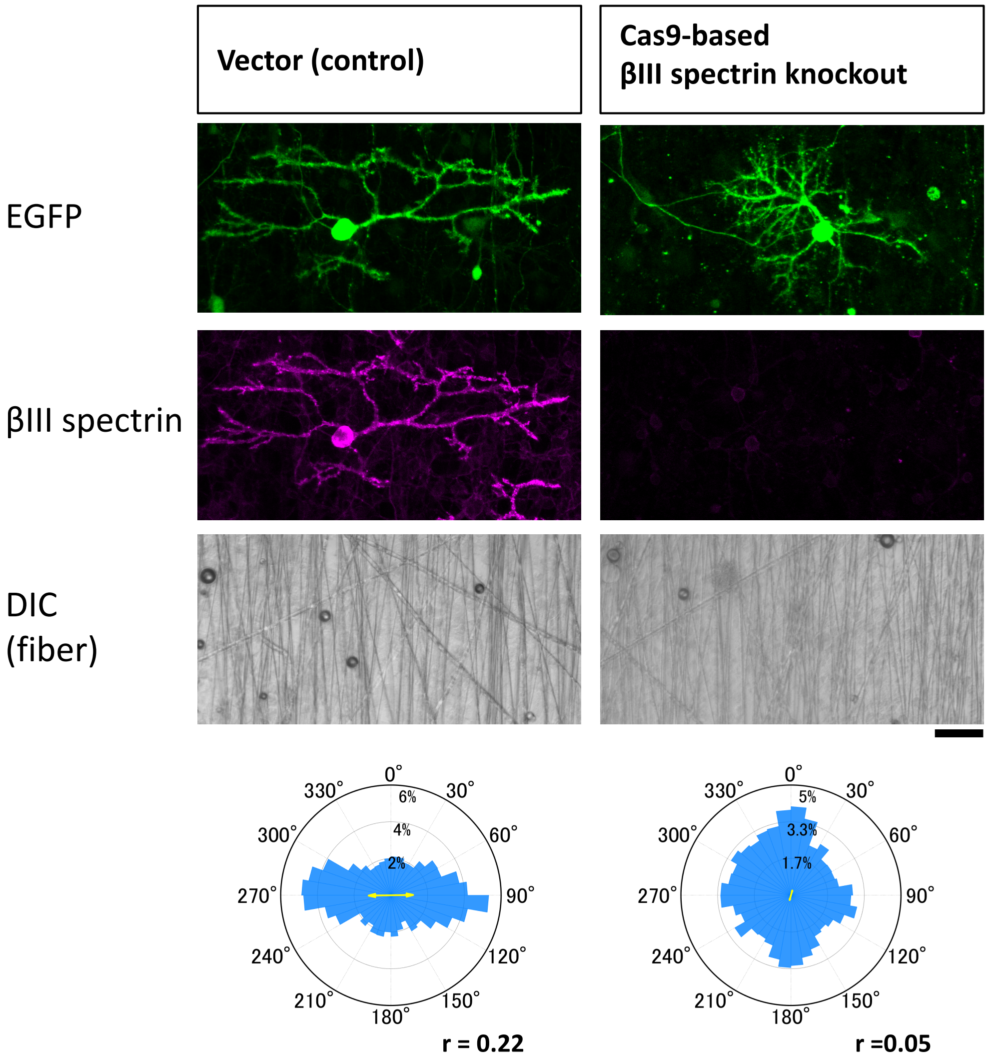

Fig. S6 CRISPR/Cas9-based βIII spectrin knockout affects the perpendicular interaction between PC dendrites and GC axons.

Representative images of PCs on aligned fibers transfected with CRISPR/Cas9 vectors (left: control empty vector, right: βIII spectrin target sequence). Cells were stained with anti-βIII spectrin (magenta). The βIII spectrin knockout cell exhibits a dendrite elongating in an abnormal orientation. n = 22 cells for control, 20 cells for βIII spectrin knockout. Scale bar: 30 µm.

Figure S7

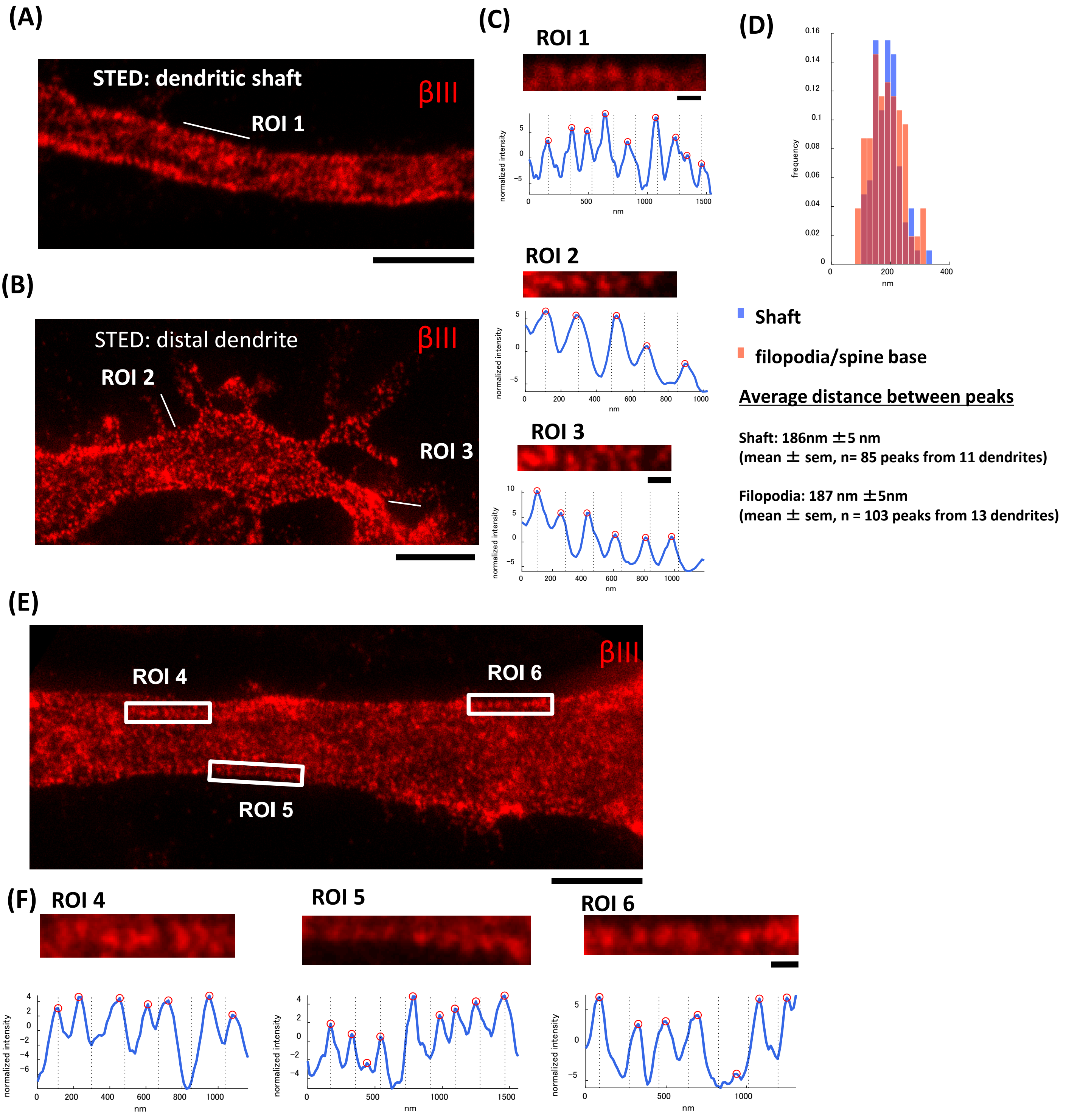

Shaft

filopodia/spine base

Average distance between peaks

Shaft: 186nm ±5 nm
(mean ± sem, n= 85 peaks from 11 dendrites)

Filopodia: 187 nm ±5nm
(mean ± sem, n = 103 peaks from 13 dendrites)

Fig. S7 Membrane periodic structure of βIII spectrin in PC dendrites

(A and B) Representative STED image of βIII spectrin in the proximal region (A) and distal region (B) of developing PC dendrites at 9-11DIV. **(C)** ROI1-3 (ROI1: dendritic shaft in (A), ROI2-3: dendritic filopodia in (B)) are magnified views. The normalized intensities of βIII spectrin repeats in ROIs 1-3 are shown by line plots below. Gray dotted lines are drawn every 185 nm from the first peak of the βIII spectrin signal. **(D)** The histogram indicates the distribution of the spacing of repeated βIII spectrin structures in the dendritic shaft (blue) and the base of dendritic protrusions (red). Shaft: n = 85 from 11 dendrites. Base of protrusions: n = 103 from 13 dendrites (dendritic base). **(E)** Another example of a STED image of βIII spectrin in the shaft region of a developing PC dendrite. **(F)** ROI4-6 are magnified views of the boxed regions in (A). Normalized intensities of βIII spectrin repeats are shown by line plots below. Scale bars: 2 µm in (A), (B), and (E). 200 nm in (C) and (F).

Figure S8

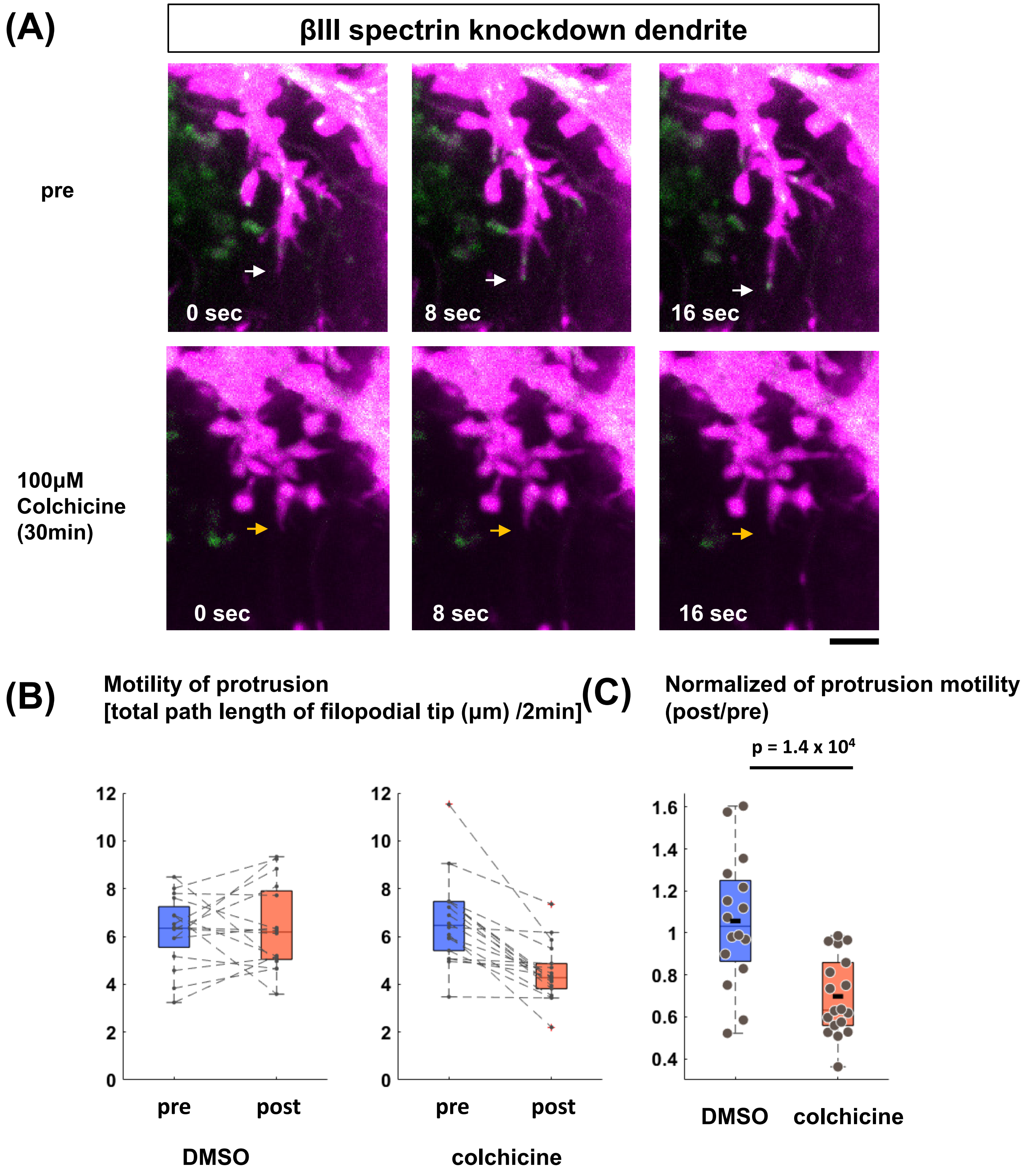

Motility of protrusion
[total path length of filopodial tip (μm) /2min]

Normalized of protrusion motility
(post/pre)

Fig. S8 Microtubule depolymerizer suppressed the protrusion motility.

(A) Representative images of protrusion extension associated with EB3-labeled microtubule polymerization in the proximal dendrite region in βIII spectrin-knockdown cells. Panels show time-series images (8-sec intervals) before (pre: top panels) and 30 min after (bottom panels) addition of 100μM colchicine. Arrows indicate the position of protrusion tips. Scale bar: 3μm. (B) Quantification of motility of protrusion in βIII spectrin-knockdown cells before (pre) and after addition of DMSO or 100μM colchicine (post, 10min-1 hr). (C) Normalized of protrusion motility comparing before and after the addition of DMSO or 100μM colchicine. Statistical test: Wilcoxon rank-sum test.

Figure S9

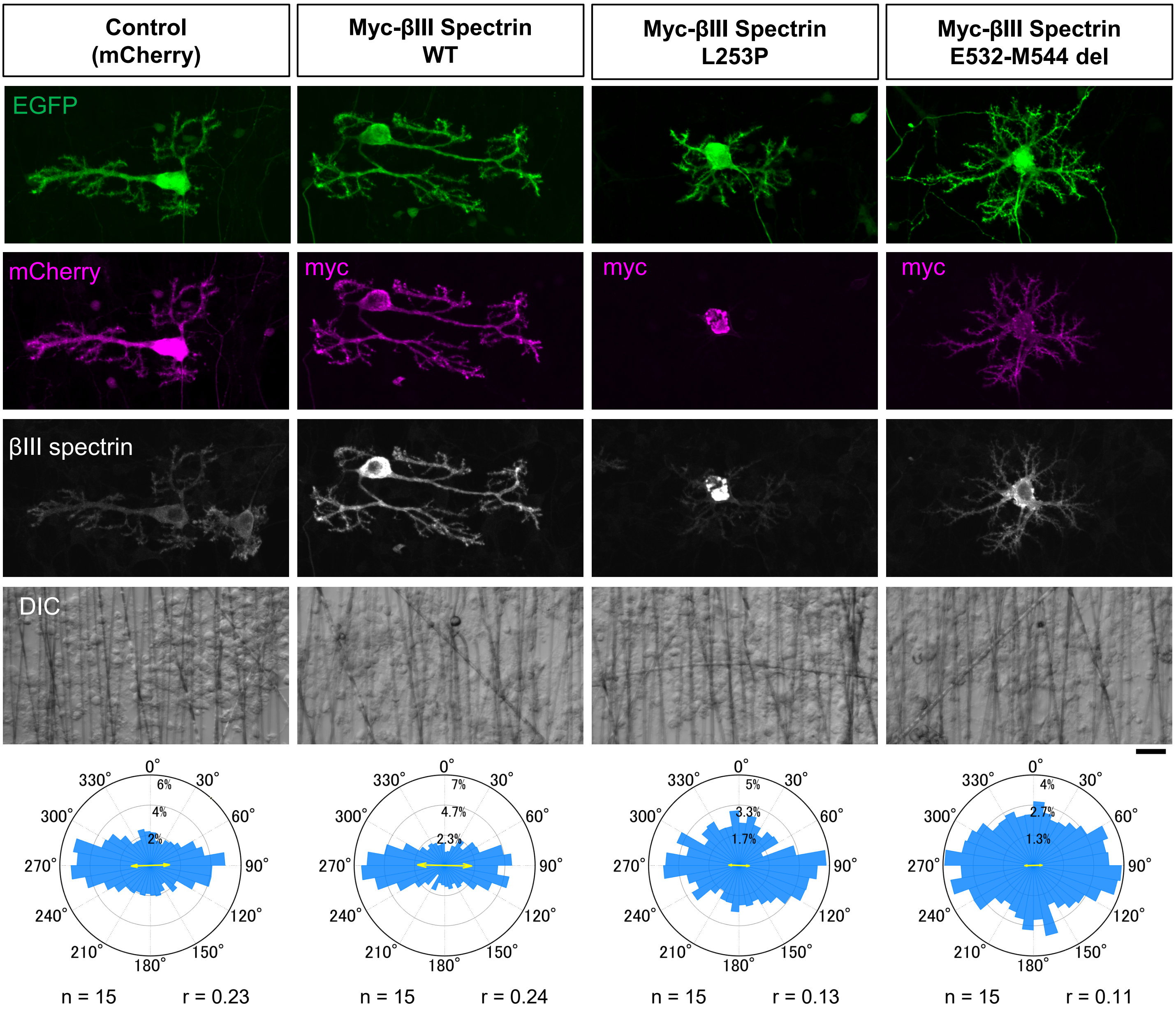

Fig. S9 L253P and E532-M544 del mutants dominantly affect dendrite arborization in wlildtype background on fiber.

Morphologies of PCs transfected with GFP plus mCherry (control), myc-tagged βIII spectrin wild-type (WT), L253P, and E532-M544 del mutant proteins grown on aligned nanofibers. Polar histograms indicate the angular distribution of dendritic segments. Scale bar: 20µm.

Table S1. Antibody list

Rabbit polyclonal anti-βIII Spectrin	SantaCruz	sc-28273
Goat polyclonal anti-βIII Spectrin	SantaCruz	sc-9660
Mouse monoclonal anti-βIII Spectrin	SantaCruz	sc-515737
Mouse monoclonal anti-αII Spectrin	SantaCruz	sc-376849
Rabbit polyclonal anti-GFP	Thermo Fisher Scientific	A-11122
Mouse monoclonal anti-GFP	Thermo Fisher Scientific	A-11120
Rabbit polyclonal anti-RFP	MBL Life Science	PM005
Mouse monoclonal anti-Calbindin	Swant	300
Mouse monoclonal anti-c-Myc	SantaCruz	sc-40
Mouse monoclonal anti-HA	Roche	1583816
Rabbit polyclonal-Pax6	Wako	019-27291
Rabbit polyclonal anti-GluD2-C	Frontier Institute	GluRD2C-Rb-Af500
Mouse monoclonal anti-tau	MERCK	MAB3420
Donkey anti-Mouse Alexa Fluor 488	Thermo Fisher Scientific	A-21202
Donkey anti-Mouse Alexa Fluor 555	Thermo Fisher Scientific	A-31570
Donkey anti-Mouse Alexa Fluor 647	Thermo Fisher Scientific	A-31571
Donkey anti-Rabbit Alexa Fluor 488	Thermo Fisher Scientific	A-21206
Donkey anti-Rabbit Alexa Fluor 555	Thermo Fisher Scientific	A-31572
Donkey anti-Rabbit Alexa Fluor 647	Thermo Fisher Scientific	A-31573
Donkey anti-Goat Alexa Fluor 555	Thermo Fisher Scientific	A-21432
Donkey anti-Goat Alexa Fluor 568	Thermo Fisher Scientific	A-11057
Donkey anti-Goat Alexa Fluor 647	Thermo Fisher Scientific	A-21447